Thesis for The Degree of Doctor of Philosophy

Hardwood Kraft Delignification

Fundamental Mechanisms at the Cell Wall Level

Linus Kron

Department of Chemistry and Chemical Engineering
Chalmers University of Technology
Gothenburg, Sweden, 2026

Hardwood Kraft Delignification
Fundamental Mechanisms at the Cell Wall Level

Linus Kron
ISBN 978-91-8103-378-6

Acknowledgements, dedications, and similar personal statements in this thesis, reflect the author's own views.

Doktorsavhandlingar vid Chalmers tekniska högskola, Ny serie nr 5835.
ISSN 0346-718X
DOI: 10.63959/chalmers.dt/5835

Department of Chemistry and Chemical Engineering
Chalmers University of Technology
SE-412 96 Gothenburg
Sweden
Phone: +46 (0)31 772 1000

Cover:
Betula pubescens, Artwork by Olivia Kron. Watercolour.

Printed by Chalmers Digitaltryck
Gothenburg, Sweden 2026.

Hardwood Kraft Delignification
Fundamental Mechanisms at the Cell Wall Level

Linus Kron

Department of Chemistry and Chemical Engineering
Chalmers University of Technology

Abstract

Kraft pulping is a globally significant industrial process whose complexity, stemming from the multi-scale heterogeneity of wood, means a complete understanding of its underlying physicochemical mechanisms remains elusive. This thesis presents research aimed at advancing the fundamental understanding of the kinetics of delignification—the primary step in kraft pulping—with a particular focus on the relative impact of reaction and transport mechanisms occurring at the cell wall level.

Delignification kinetics were investigated in laboratory-scale reactors by examining the effects of time, temperature, and cooking liquor composition on pulp and dissolved component properties. The work focused primarily on birch wood meal but also included comparisons with wood chip pulping and other Nordic hardwood species, namely alder, aspen, and beech. Based on the experimental findings, a novel delignification model incorporating both reaction and diffusion phenomena was developed.

Collectively, the studies highlight the multi-mechanistic nature of kraft delignification, indicating that different phenomena dominate the kinetics at different stages of the process. The results demonstrate that the sulphide dependency of the delignification rate diminishes part-way through the process, indicating the impact of additional reactions not previously considered to significantly influence the delignification rate. In contrast, the molecular size of dissolved lignin was observed to increase continuously throughout cooking, suggesting that solubility and diffusion effects significantly impacts the later stages of lignin removal. The developed model demonstrated that delignification kinetics in wood meal pulping can be accurately represented as primarily diffusion controlled. Finally, delignification of wood chips revealed additional heterogeneity at a larger length scale. An initial extension of the developed delignification model to the chip scale successfully captured this behaviour, indicating that accounting for alkali availability is critical to accurately describe delignification in chips.

Keywords

Pulping, Wood meal, Black liquor, Lignin, Model, Reaction, Transport

List of publications

This thesis is based on the work contained in the following papers:

Paper I **A comparative study of delignification behaviour during kraft pulping of four Nordic hardwoods**
Linus Kron, Merima Hasani, Hans Theliander.
Holzforschung, 78, 2024, 434-445

Paper II **On the mechanistic and kinetic role of hydrogen sulphide during kraft delignification**
Linus Kron, Merima Hasani, Hans Theliander.
Manuscript, submitted

Paper III **Kraft cooking of birch wood chips: differences between the dissolved organic material in pore and bulk liquor**
Linus Kron, Carolina Marion de Godoy, Merima Hasani, Hans Theliander.
Holzforschung, 77, 2023, 598-609

Paper IV **Heterogenous Diffusion and Reaction Model of Kraft Delignification at the Cell Wall Level**
Linus Kron, Merima Hasani, Hans Theliander.
Industrial and Engineering Chemistry Research, 64, 2025, 1497-1507

Paper V **1D Multiscale modelling of delignification rate in hardwood chips during kraft pulping**
Carolina Marion de Godoy, Linus Kron, Merima Hasani, Hans Theliander.
Manuscript, submitted

Contribution report

Paper I **Main author**. Responsible for planning and conducting all experimental work, except running the NMR measurements. Results were evaluated together with co-authors. Responsible for drafting the manuscript, revised together with co-authors.

Paper II **Main author**. Responsible for conceptualizing the study, planning and conducting all experimental work, except running the NMR measurements. Results were analysed together with co-authors. Responsible for drafting the manuscript, revised together with co-authors.

Paper III **Shared first authorship** with CMdG. Both first authors were responsible for planning and conducting all experimental work, except running the NMR measurements. Results were analysed together with co-authors. Both first authors were responsible for drafting the manuscript, revised together with co-authors.

Paper IV **Main author**. Responsible for conceptualizing the study, planning and conducting all experimental work, and developing the model. Results were evaluated together with co-authors. Responsible for drafting the manuscript, revised together with co-authors.

Paper V **Shared first authorship** with CMdG. Both first authors were responsible for extending the model initially developed by LK, based on the experimental data procured by CMdG. Results were analysed together with co-authors. Both first authors were responsible for drafting the manuscript, revised together with co-authors.

Conferences

Parts of this work has also been presented at the following occasions:

I **Hardwood Delignification: Influence of Impregnation**
Carolina Marion de Godoy, Linus Kron, Merima Hasani, Hans Theliander
16^{th} European Workshop on Lignocellulosics and Pulp
Gothenburg, Sweden, June 2022
Poster

II **Kraft Cooking of Birch: Pore and Bulk Liquor Composition.**
Linus Kron, Carolina Marion de Godoy, Merima Hasani, Hans Theliander
21^{st} International Symposium on Wood, Fiber, and Pulping Chemistry
Venice, Italy, July 2023
Poster

III **Comparative Analysis of Hardwood Kraft Delignification: Insights from the Black Liquor Composition**
Linus Kron, Merima Hasani, Hans Theliander
Paper & Biorefinery Conference & Tradeshow
Graz, Austria, May 2024
Oral presentation

IV **Hardwood Kraft Delignification**
Linus Kron, Merima Hasani, Hans Theliander
Ekmandagarna — The Gunnar Sundblad session for young researchers
Stockholm, Sweden, January 2025
Oral presentation

V **Revisiting Kraft Delignification – Modelling the Heterogenous Removal of Lignin at the Cell Wall Level**
Linus Kron, Merima Hasani, Hans Theliander
22^{nd} International Symposium on Wood, Fiber, and Pulping Chemistry
Raleigh, USA, June 2025
Oral Presentation

VI **The Kinetics of Kraft Delignification - Insights Gained from a Heterogeneous Modelling Approach**
Linus Kron, Merima Hasani, Hans Theliander
WWSC International Conference
Stockholm, Sweden, June 2025
Poster

VII **Hardwood Delignification – Understanding Chemistry and Mass Transport Fundamentals**
Linus Kron, Merima Hasani, Hans Theliander
MWP Symposium — Young Researcher's Challenge
Stockholm, Sweden, November 2025
Poster and Oral presentation

Abbreviations

ASL	Acid-soluble lignin
BL	Bulk cooking liquor
CL	Centrifuged cooking liquor
DP	Degree of polymerisation
ECCSA	Effective Capillary Cross-Sectional Area
GPC	Gel Permeation Chromatography
HPAEC-PAD	High Performance Anion Exchange Chromatography with Pulsed Amperometric Detection
HSQC-NMR	Hetero-nuclear Single Quantum Coherence Nuclear Magnetic Resonance spectroscopy
IS	Ionic strength
MeGlcA	4-O-methylglucuronic acid
M_W	Weight-average molecular weight
MWD	Molecular weight distribution
odw	Oven-dry Wood
PEG	Polyethylene glycol
RI	Refractive index
S/G	Syringyl to Guaiacyl ratio
UV	Ultraviolet light

Symbols

A_r	Frequency factor of reaction rate constant $[s^{-1}]$
D_0	"Base diffusivity" analogous to the frequency factor A_r $[m^2/s]$
D_L	Diffusivity of dissolved lignin A_r $[m^2/s]$
D_{OH}	Diffusivity of OH^- A_r $[m^2/s]$
E_D	Activation energy of lignin diffusivity $[J]$
E_r	Activation energy of reaction rate constant $[J]$
L_{D_i}	Relative mass concentration of dissolved/reacted lignin, fraction $i = [1, 2, , 7]$, $[-]$
L_S	Relative mass concentration of solid/unreacted lignin $[-]$
M	Number of layers at the cell wall scale $[-]$
m	Order of the OH^- dependence of the diffusivity $[-]$
N	Number of segments at the wood chip scale $[-]$
r_H	Hydrodynamic radius $[m]$
r_L	Reaction rate of solid lignin $[s^{-1}]$
w_i	Relative weight of dissolved lignin $i = [1, 2, , 7]$, $[-]$

Contents

Till mamma och pappa

Preface

As a child, I once exclaimed: "*When I grow up, I'm gonna do research.*"
The topic was a bit unclear, but it involved forest fires, ants, and deer. And, in a way, I did follow through: I have now spent many days subjecting wood to heat and sulphur—basically like the fires of hell, but in a fume hood.
Fortunately, no animals were involved.

I would like to think I still maintain the same curiosity today. Back then, the answer to a single question was—sometimes to my parents' frustration—often met with two more questions. Some twenty-odd years later, attempting to understand kraft delignification has not improved the situation. Only now it is, frustratingly, *I* who must answer all of these questions. Worse still, I am not even sure how many answers I have actually managed to procure during my years as a PhD student, yet the questions keep piling up.
Apparently, this is the meaning of true research (or so my ever-supporting supervisors assure me).

27$^{\text{th}}$ of February 2026, Gothenburg

Chapter 1

Introduction

Mitigating the irreversible impacts associated with global climate change requires a transition towards sustainable and circular economic systems [1]. Central to this transition is a substantial reduction in the reliance on fossil-based raw materials, accompanied by the increased utilisation of renewable, bio-based alternatives. Lignocellulosic biomass derived from trees and plants represents the most abundant source of such renewable feedstocks, positioning the pulp and paper sector as a key contributor to the emerging bio-based economy. When integrated into biorefinery concepts, existing pulping technologies enable the production of a broad range of materials, including textiles, packaging, speciality chemicals, and pharmaceutical components [2]. However, despite the large global availability of lignocellulosic resources, the supply remains finite, making the efficient utilisation of all biomass components essential for a sustainable process industry.

At present, the kraft pulping process dominates the industrial separation of wood components. A central operation in this process is the delignification, during which lignin and part of the hemicelluloses are removed to liberate cellulose-rich fibres for subsequent applications. In modern kraft mills, the overall pulp yield is typically around 50%, as lignin and hemicelluloses are extensively solubilised during cooking. Although these dissolved components account for approximately half of the original wood mass, they are largely underutilised for material applications and are instead predominantly burned for energy recovery. This situation arises in part from the difficulty of extracting intact cellulose fibres without extensive degradation of the other wood components [3]. Improving resource efficiency therefore requires a deeper understanding of the fundamental mechanisms governing pulping, both to enhance fibre yield and to enable the development of novel bio-based materials capable of replacing fossil-derived products.

The delignification itself is a highly complex process involving concurrent chemical reactions of lignin and carbohydrates alongside the transport of reactants and dissolved species through the porous wood structure. The inherent het-

erogeneity of wood, comprising fibres and pore networks with varying size, orientation, and connectivity, further complicates this picture. Moreover, the internal structure of the wood matrix is continuously altered as delignification proceeds, influencing both transport pathways and reaction environments [4]. To manage this complexity, many delignification models adopt simplified descriptions that isolate a limited number of dominant mechanisms. In most cases, the process is treated as pseudo-homogeneous, with overall kinetics assumed to be governed primarily by the rate of bond cleavage within the lignin macromolecule [5].

Accumulating evidence, however, indicates that reaction kinetics alone are insufficient to describe delignification behaviour. It has long been recognised that excessive chip thickness leads to non-uniform pulping [6, 7], an effect commonly attributed to restricted transport of cooking chemicals into the chip interior. Such spatial non-uniformity also influences the behaviour of dissolved lignin, although its impact on delignification kinetics has only attracted focused attention in more recent studies [8–10]. In addition, transport limitations have been suggested to extend beyond the chip scale and, under certain conditions, to occur within the fibre cell wall itself [11, 12]. Despite these observations, only a limited number of delignification models explicitly incorporate the transport of wood components [9, 13–15]. Those that do typically rely on simplified transport descriptions that neglect the heterogeneous chemical nature of lignin and its influence on transport properties. As a result, the relative roles of transport and reaction phenomena during kraft delignification remain incompletely understood, underscoring the need for continued investigation in this area.

1.1 Objectives

The main objective of this work has been to advance the understanding of the kinetics of kraft delignification by investigating the relative impact of the reactions and transport of lignin. Specifically, this objective has been pursued through the following sub-objectives:

1. To investigate kraft delignification kinetics at the cell wall level through the pulping of wood meal, and how it varies depending on the:
   (a) Process conditions, such as time, temperature, and liquor composition.
   (b) Tree species, comparing birch with other Nordic hardwoods.
2. To develop a model for describing the heterogenous delignification at the cell wall level.
3. To perform complementary comparisons with wood chip pulping.

This thesis summarises the work conducted across five individual studies, which address the following topics:

Paper 1

- Topic: Variation in time and temperature
- Material: Wood meal of four Nordic hardwoods

Paper 2

- Topic: Variation in sulphide levels
- Material: Birch wood meal

Paper 3

- Topic: Comparison of bulk and lumen liquor
- Material: Birch wood chips

Paper 4

- Topic: Numerical modelling of delignification kinetics
- Material: Birch wood meal

Paper 5

- Topic: Numerical modelling of delignification kinetics
- Material: Birch wood chips

1.2 Outline of the thesis

Chapter 2 and 3 provide brief overviews of the chemistry and structure of wood, and of kraft delignification chemistry, respectively. Chapter 4 describes the materials, equipment, and methodology employed in this work, while chapter 5 presents the main findings of the appended papers. Finally, chapter 6 summarises the conclusions of the thesis and outlines some recommendations for future research in the field.

Chapter 2

Wood

This chapter briefly outlines the structural and chemical features of wood and its constituent macromolecules.

2.1 Morphology

Wood exhibits a complex, hierarchical structure composed of a heterogeneous network of cells, broadly categorized into softwood (derived from gymnosperms) and hardwood (derived from angiosperms). In softwoods, longitudinal tracheids constitute approximately 95% of the structure, serving the dual function of mechanical support and fluid transport. Conversely, hardwoods employ specialized cell types for these roles: vessels facilitate longitudinal fluid transport, while libriform fibres and fibre tracheids provide structural support. Although both wood types contain radially distributed parenchyma cells for nutrient storage, softwoods additionally possess tracheid rays to manage radial fluid transport [16]. Morphologically, hardwood fibres are generally characterized by shorter lengths, narrower widths, and thicker cell walls relative to softwood tracheids [17], with some typical values presented in Table 2.1

Table 2.1: Typical dimensions of some softwood and hardwood fibres [18].

	Length [mm]	Width [μm]	Wall thickness [μm]
Softwood			
Spruce *(Picea abies)*	3.5	27	2.9
Pine *(Pinus sylvestris)*	2.9	28	3.2
Hardwood			
Birch *(Betula pendula)*	1.1	20	1.9
Beech *(Fagus sylvatica)*	1.5	14	3.3

The cell walls of both tracheids and hardwood fibres are arranged in a multi-layered structure defined by varying orientations of cellulose fibrils, as illustrated in Figure 2.1. The outermost primary cell wall is thin and features a random fibril arrangement. Inside of this lies the secondary cell wall, which is subdivided into three distinct layers: S1, S2, and S3, with the S2 layer being the dominant section, accounting for 70–80% of the total wall thickness [17]. While the S1 and S3 layers contain fibrils oriented in counter-running helices, the S2 layer is characterized by a predominantly vertical fibril alignment, although the microfibril angles significantly varies, depending on the wood's maturity (juvenile versus mature) and the presence of environmental stress (e.g. reaction wood). The liquid-filled cavity within the fibre is called the lumen, which via connections between adjacent fibres (called pores) comprises a network that facilitates transport of nutrients—and in the context of pulping, cooking chemicals—within the wooden matrix. Bonding adjacent fibres together is the lignin-rich middle lamella.

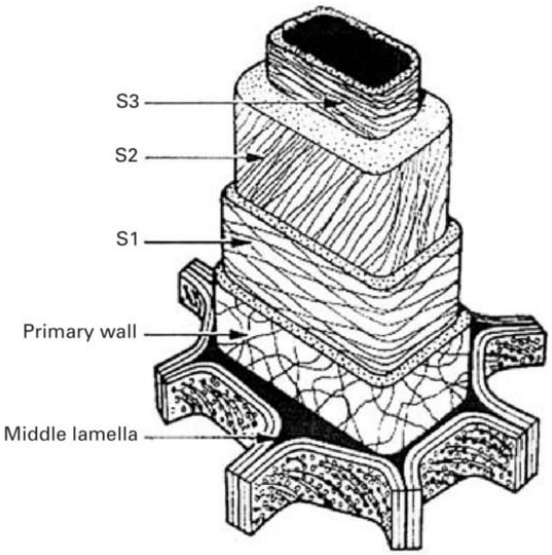

Figure 2.1: Schematic drawing of a wood fibre cell wall. CC BY [19].

2.2 Chemical structure

The chemical composition of wood is primarily defined by three major macromolecular groups: cellulose, lignin, and hemicelluloses. In addition, wood also contains a diverse fraction of low molecular weight compounds collectively referred to as *extractives*. This category encompasses substances such as fatty acids, sterols, and terpenes. Quantitative analysis indicates that extractives generally constitute a minor proportion of the material, ranging from less than 1% up to 5% of the total wood mass [20].

2.2.1 Cellulose

As the most abundant biopolymer on Earth, cellulose serves as the fundamental structural component of wood biomass. Chemically, it is defined as a linear homopolysaccharide composed of β-D-glucose units connected via $1 \rightarrow 4$ glycosidic linkages (Figure 2.2). Native cellulose typically exhibits a degree of polymerization ranging from 7000 to 15000 [17]. The equatorial orientation of hydroxyl groups on the glucopyranose rings imparts amphiphilic characteristics to the polymer chains, facilitating extensive intra- and intermolecular hydrogen bonding, and amphiphilic association. These interactions drive the assembly of supramolecular structures, where intramolecularly β-glycosidic bonded sheets stack to form crystalline domains interspersed with less ordered regions. However, the precise distinction between—and definition of—these crystalline and disordered regions remains a subject of discourse within the field [21]. This hierarchical arrangement produces elementary fibrils, which in turn aggregate into microfibril bundles with widths approximating 15 to 20 nm [22]. Within the cell wall matrix, these bundles interact with hemicelluloses and lignin to form macrofibrils, establishing the primary structural framework of wood, illustrated as the distributed lines in Figure 2.1.

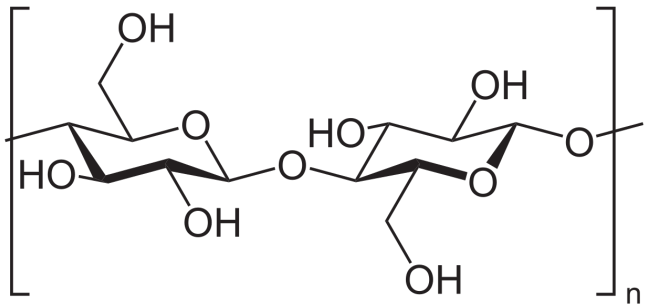

Figure 2.2: A cellobiose unit: the smallest repeating unit of cellulose.

2.2.2 Hemicelluloses

In contrast to the homopolymeric structure of cellulose, hemicelluloses represent a heterogeneous class of polysaccharides characterized by distinct monomeric compositions, branching patterns, and functional group substitutions. The primary monosaccharide constituents include glucose, mannose, xylose, galactose, and arabinose. Within wood matrices, these polymers predominately exist as (galacto)glucomannan and (arabino)glucuronoxylan (Figure 2.3). As opposed to cellulose, these backbones may be branched or contain side groups; for instance, O-acetyl groups frequently substitute the main chain, typically occurring in the absence of arabinose units. Additionally, (arabino)glucuronoxylan is distinguished by substitutions with 4-O-methylglucuronic acid (MeGlcA). Relative to cellulose, hemicelluloses exhibit a considerably lower degree of polymerization, typically between 100 and 200 [17]. While their full biological function requires further elucidation, hemicelluloses are posited to reinforce the cell wall through their linear backbones. Furthermore, research suggests they

act as coupling structures between lignin and cellulose, thereby influencing the structural arrangement and crystallinity of cellulose fibrils [23].

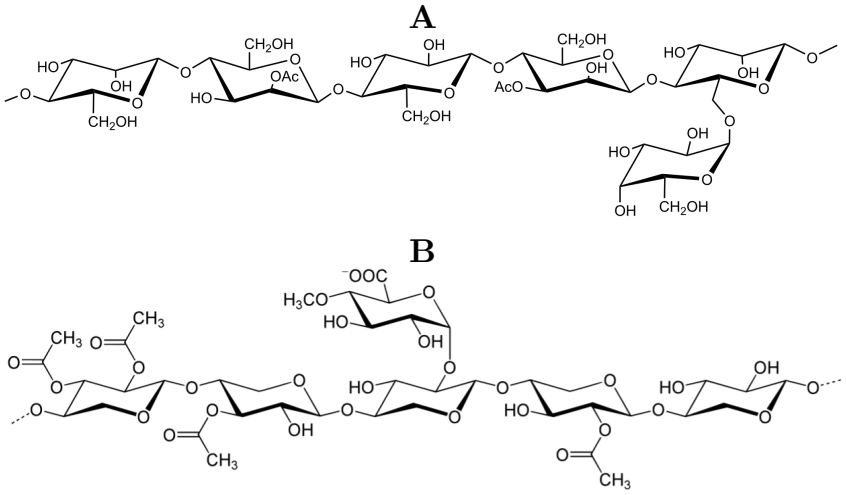

Figure 2.3: Schematic representations of hemicelluloses. (A) A glucomannan polymer with a galactose substituent. (B) A xylan polymer with a 4-O-MeGlcA. Both polymers contain acetyl groups.

2.2.3 Lignin

As the second most prevalent component of wood biomass, lignin fulfils essential structural and protective functions. It ensures cell wall integrity, acts as an inter-fibre binder, promotes hydrophobicity for water transport, and contributes to microbial resistance [24]. Lignin is unevenly distributed across the cell wall, with concentrations ranging from about 20% in the S2 layer to more than 80% in middle lamella corners in some species. Despite its lower local concentration, approximately 70% of the total lignin content is found in the S2 layer due to its considerable thickness [4]. Chemically, lignin differs fundamentally from polysaccharides like cellulose; rather than a linear chain, it is an amorphous, three-dimensional macromolecule formed through the irregular cross-linking of phenylpropane units via ether and carbon-carbon bonds [25]. The polymer is derived from three primary monolignol precursors: p-coumaryl alcohol, coniferyl alcohol, and sinapyl alcohol (Figure 2.4). Within the lignin network, these precursors are typically referred to by their corresponding C–6 units: p-hydroxyphenyl (H), guaiacyl (G), and syringyl (S), respectively.

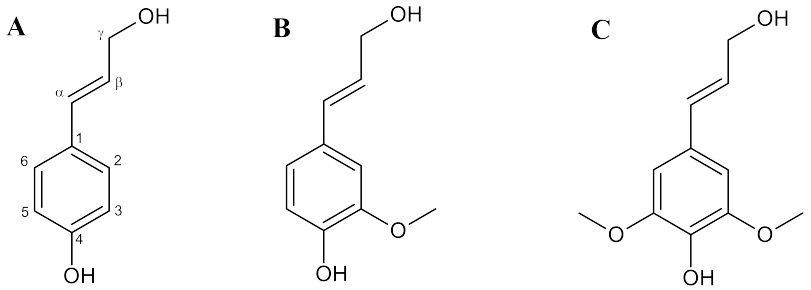

Figure 2.4: Structure of the three monolignols (A) p-coumaryl alcohol, (B) coniferyl acohol, and (C) sinapyl alcohol. Conventional naming of the C atoms is indicated in Structure A.

Figure 2.5 illustrates some of the major inter-unit linkages in the lignin network. Aryl ether bonds are the most prevalent, with β-O-4 and the comparatively minor α-O-4 structures together comprising about 50–60% of all inter-unit bonds. The remaining structural framework is composed of carbon-carbon and ether linkages, including β-5, 5-5', and β-1', each of which constitute 5–10% of the total bond distribution [4, 17, 24].

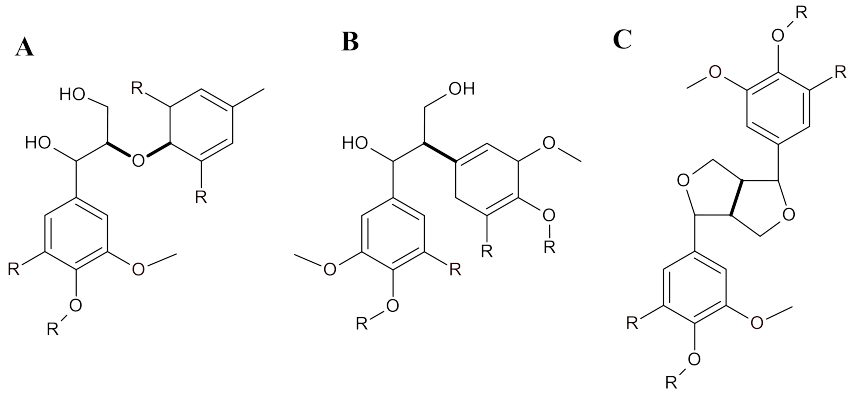

Figure 2.5: Schematic representation of three common inter-lignin linkages, with the relevant bond highlighted with bold lines: (A) β-O-4, (B) β-1, and (C) β-β.

Nevertheless, elucidating the precise structure of native lignin presents significant analytical challenges, primarily because its inherent recalcitrance necessitates isolation protocols that inevitably alter its chemical composition [26, 27]. Historically, the milled-wood lignin (MWL) protocol established by Björkman [28]—which involves extensive ball-milling followed by dioxane extraction—has been regarded as yielding lignin with a relatively intact structure, and is therefore often described as a *native-like* lignin. Subsequent methodological advancements have integrated enzymatic and acidolytic treatments to substantially enhance extraction yields [29, 30]. Despite these optimizations, a universal standard for lignin isolation is currently lacking. The continued application of diverse methodologies results in significant variations in the reported data, thereby complicating structural comparisons across the literature [31]. In

addition to these native-like lignins, technical lignins recovered from industrial process streams—and which are of significant economic interest—are equally dependent on their extraction procedures. Moreover, these materials also diverge chemically from their native precursors; typically, they contain reduced concentrations of aliphatic hydroxyl groups and β-O-4 linkages, alongside an increased frequency of phenolic hydroxyl groups and condensed carbon-carbon bonds [32, 33].

For similar reasons, estimations of the molecular weight of native lignin is inherently troublesome. For native-like lignin the weight-averaged molecular weight (M_W) is typically reported to be 10–30 kDa [25, 34, 35], although the range of reported values spans 3-300 kDa [17, 36]. Technical lignins vary considerably depending on the method of pulping and separation [17]. Kraft lignins are typically smaller at 3–15 kDa [10, 17, 32], but has also been reported as significantly larger fractions [37, 38], whereas lignosulfonates have been reported at several hundreds of kDa [17].

2.2.4 Differences between softwood and hardwood

Softwood

While Section 2.1 delineated the morphological distinctions between wood categories, their chemical compositions also diverge significantly. In softwoods, glucomannan is the dominant hemicellulose, characterized by varying substitution with galactose and acetyl groups. Arabinoglucuronoxylan occurs in lesser proportions, where the concentration of mannose units is roughly double that of xylose [17]. Softwood lignin is primarily composed of guaiacyl units (up to 95%), with minor contributions from p-hydroxyphenyl units. Due to the absence of syringyl units, it is occasionally referred to as *G-lignin*.

Hardwood

In contrast to the relative uniformity of softwoods (with the notable exception of larch), hardwoods display greater chemical heterogeneity. The primary hemicelluloses are glucuronoxylans, which are distinguished by a lack of arabinose side groups and a lower frequency of MeGlcA substitution compared to their softwood counterparts. Glucomannans are present in lower concentrations and lack the galactose substituents found in softwoods. Moreover, the polymer backbone of hardwood hemicelluloses exhibits a high degree of acetylation at the C2 and C3 positions [17]. Hardwood lignin comprises a mixed composition of syringyl and guaiacyl moieties, with the S/G ratio typically ranging from 1:2 to 4:1. This compositional difference influences the linkage distribution; hardwoods contain a higher proportion of non-condensed β-O-4 linkages, whereas softwoods are richer in condensed structures such as β-5 and 5-5' bonds [24].

Table 2.2: Reported distributions of chemical components in different tree species. Reprinted with permission [48].

Species	Glc	Man	Xyl	Ara	Gal	Klason	ASL[a]	Extractives	References
Black alder	48.1[b]	-[b]	31.9[b]	-[b]	-[b]	19.9[c]	-[c]	-	[39]
Alnus glutinosa	50.9[b]	-	-	-	-	21.8[c]	-[c]	4.9	[40]
	43.4[b]	-[b]	23[b]	-[b]	-[b]	23.9[c]	-[c]	3.8	[17]
Silver birch	46.5	2.0	26.7	0.6	1.2	19.6	-	-	[41]
Betula pendula[d]	44.5	2.1	23.6	0.7	0.8	21.5	-	2.24	[42]
	37.4	1.5	20.3	0.3	0.5	19.6	3.1	-	[43]
	41.0[b]	2.3[b]	27.5	-	-	22.0[c]	-[c]	3.2	[4]
	34.2[b]	4.8[b]	32.5[b]	-	1.7	26.3[c]	-[c]	-	[17]
Betula pubescens[e]	42.2[b]	-	-	-	-	19.2	0.76	2.1	[44]
European beech	39.4[b]	1.3[b]	27.8[b]	-	-	24.8[c]	-[c]	1.2	[4]
Fagus sylvatica	42.9[b]	5.2[b]	23.0[b]	1.9[b]	-[b]	23.4	1.1	0.0	[45]
	43.3[b]	1.4[b]	27.8[b]	-	2.6	24.4[c]	-[c]	-	[17]
	49.1[b]	-[b]	22.0[b]	-[b]	-[b]	23.8[c]	-[c]	0.8	[17]
	44.5[b]	-[b]	20.6[b]	-[b]	-[b]	22.2[c]	-[c]	-	[17]
European aspen	41.1	3.9	16.7	0	0	19.3	2.9	-	[46]
Populus tremula	51.1	2.6	22.9	0.5	0.6	21.7[c]	-[c]	-	[47]
	51.2	2.3	22.7	0.6	0.7	19.3	-	-	[41]
Norway spruce	41.7[b]	16.3[b]	8.6[b]	3.4[b]	-[b]	27.4[c]	-[c]	1.7	[4]
Picea abies	44.9[b]	14.7[b]	8.2[b]	1.1[b]	-[b]	28.2	0.8	-	[45]

[a] Acid-soluble lignin. [b] Data reported as cellulose/glucomannan/xylan. [c] Data reported as total lignin (both ASL and Klason). [d] *B. pendula* is also known as *B. verrucosa*. [e] English name: Downy birch

Chapter 3

Kraft delignification

This chapter summarises the dominant chemical mechanisms governing the main delignification step during kraft pulping, followed by a review of their effect on the delignification kinetics.

The manufacture of paper and board products requires rigorous conversion of wood biomass into pulp. Modern pulping operations generally follow a standardized sequence: logs are initially debarked and cut into wood chips. Following potential pre-treatment, these chips enter the primary defibration stage, where individual fibres are liberated via mechanical action and/or chemical treatment. Subsequent processing steps, including washing and—when desirable—multi-stage bleaching, are employed to tailor the pulp's final properties, particularly regarding brightness and residual lignin content [49]. Among available technologies, the kraft process is the predominant method; originating in the late 19th century, it currently constitutes over 80% of the global pulp production [50].

3.1 Mechanisms

The fundamental objective of the kraft process is delignification, which entails the solubilization and extraction of up to 85% of the initial lignin content to achieve fibre liberation. This is not a singular chemical event but rather a composite process governed by interacting reaction and mass transfer mechanisms. The overall progression can be deconstructed into a sequence of key steps:

1. External mass transport of active cooking chemicals from the bulk liquor to the wood chip surface.
2. Internal transport of chemicals from the chip surface to the cell wall interface via the capillary network of lumens.
3. Diffusion of chemicals into the fibre wall to reach reactive sites.
4. Chemical fragmentation of bonds within the macromolecular network.

5. Solubilization of the fragmented wood components.
6. Diffusion of dissolved components from the reaction sites to the cell wall surface.
7. Internal transport of dissolved components through the lumen network to the chip exterior.
8. External transport of dissolved components from the chip surface into the bulk liquor.

While this scheme outlines the theoretical requirements for delignification, the actual process dynamics are influenced by several concurrent factors. For instance, side reactions involving carbohydrates—specifically hydrolysis, peeling, and deacetylation—compete for the supply of active chemicals, thereby reducing the reactant concentration available for lignin fragmentation [51]. Furthermore, the accumulation of dissolved degradation products modifies the physicochemical environment of the liquor, including its ionic strength, which subsequently may influence both reaction rates and transport mechanisms [52]. In addition, the natural structural variability of the wood matrix creates significant challenges when attempting to isolate and quantify the individual contributions of these kinetic and diffusion-controlled steps. Evidently, delignification is truly a complex process, which warrants proper consideration of all underlying mechanisms.

3.1.1 Reactions

Lignin

Lignin solubilization necessitates reactions which reduce molecular weight and incorporate hydrophilic moieties. These changes are achieved principally through the cleavage of ether bonds, as carbon-carbon linkages exhibit significant stability. Consequently, the scission of the abundant β-O-4 linkage constitutes the primary fragmentation reaction. The specific mechanism is dictated by the presence of a phenolic group at the C4 position. In phenolic structures, alkaline conditions induce the formation of a quinone methide intermediate, which may be subjected to a nucleophilic attack by HS^- ions to cleave the interunit linkage (see Figure 3.1). Conversely, in non-phenolic structures the quinone cannot form, and instead β-O-4 cleavage proceeds on a path essentially independent of HS^-, requiring only OH^-. Both pathways generate new phenolic groups, potentially sustaining the reaction chain in subsequent ether linkages [4].

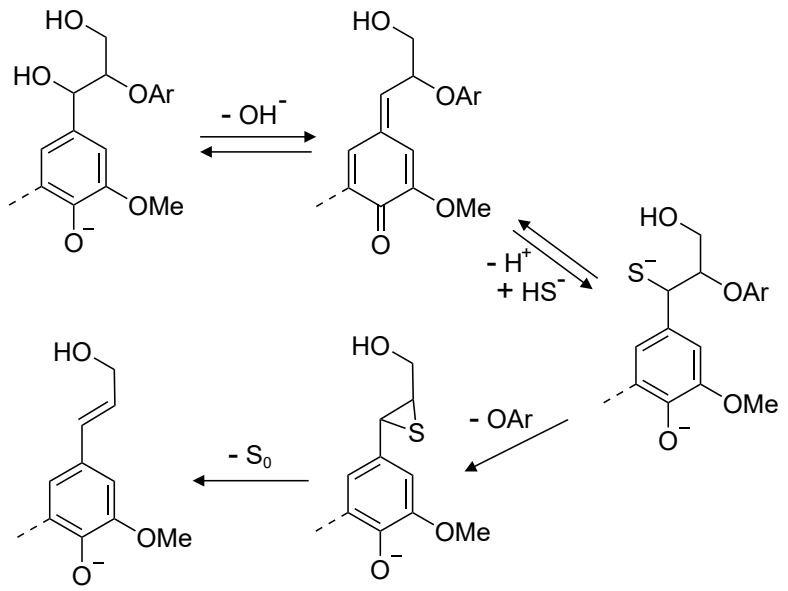

Figure 3.1: Schematic reaction pathway of the sulfidolytic β-O-4 cleavage in phenolic structures at kraft conditions.

HS^- also participates in the demethylation of the C3 and C5 methoxy groups, introducing phenolic functionalities without affecting interunit linkages, as shown in Figure 3.2. Apart from these reactions, few other interactions between lignin and HS^- have traditionally been considered (with the exception of thiolignin intermediates) [4, 53]. However, it has been proposed that sulphur can act as an electron acceptor in radical-induced polymerisation reactions [54], which may impede delignification if such re-polymerisation occurs to an extent that reduces solubility.

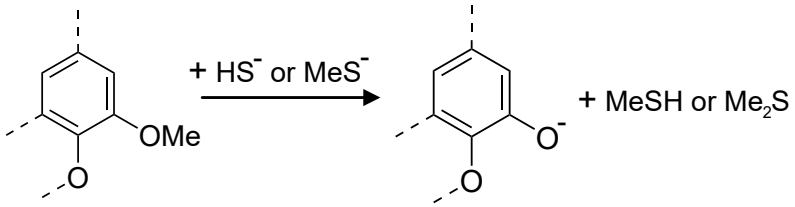

Figure 3.2: Schematic reaction pathway of the sulfidolytic demethylation.

A similar class of carbon–carbon bond-forming condensation reactions, although independent of HS^-, has long been considered to limit the final stages of delignification [55]. These structures occur at increased concentrations in the lignin remaining in the pulp after cooking and are generally assumed to form predominantly at the 5-position of guaiacyl units, although no conclusive mechanistic pathway has been established [56]. However, it is also possible that such condensed units are not generated during cooking but instead become enriched in the residual lignin as other, more labile structures are preferentially degraded and dissolved [57, 58]. In addition, certain condensed linkages more common in hardwoods, such as α–5 bonds, have been reported to be more abundant in the dissolved lignin than in the residual fraction [56].

Other reactions occurring during alkaline pulping include the formation of alkali-stable enol ethers from phenolic β-O-4 linkages. These reactions initiate with same quinone methide intermediate as for the cleavage reaction (c.f Figure 3.1), but then proceeds via an alternative pathway independently of HS^-. As this alternative pathway competes with the cleavage reaction for the quinone methide, it may therefore hinder delignification when sulfidity—and correspondingly the rate of the cleavage reaction—is low [59]. Related pathways may take place in condensed β-1 or β-5 structures, where a similarly stable stilbene structure is formed instead of an enol ether. Neither reaction contributes to depolymerisation, as they do not cleave the lignin backbone. However, the conjugated intermediates that is formed may undergo base-catalysed retrograde aldol reactions that do cleave the backbone, although this accounts for only a minor fraction of total lignin chain scission [55].

Carbohydrates

Carbohydrate degradation during kraft pulping is primarily driven by two mechanisms: peeling and alkaline hydrolysis, though reactions involving functional side groups also play a role. Under alkaline conditions and intermediate temperatures (>70°C), polysaccharide chains undergo β-elimination at the reducing end. This stepwise depolymerization, termed the peeling reaction, propagates until a competing stopping reaction generates a chemically stable end-group [56]. Cellulose is affected to a limited extent, partly because its high degree of polymerization (DP) implies fewer reducing end groups per monomer unit, but also because the crystalline regions provide limited accessibility for alkali to initiate the reaction. In contrast, glucomannans, having lower DP and greater accessibility, suffer substantial yield loss from peeling. Xylans, on the other hand, exhibits partial stability; xylose units substituted with MeGlcA or arabinose units (in softwoods) at the C2 and C3 positions promotes the stopping reaction [60]. Moreover, xylan is potentially also aided through association with cellulose, reducing its accessibility [61].

At elevated temperatures (>140°C), alkaline hydrolysis becomes substantial, characterized by the random cleavage of glycosidic bonds. For cellulose, this reaction preferentially targets less ordered regions and constitutes the primary cause of DP reduction during pulping [56]. Crucially, hydrolysis generates new reducing end groups, which subsequently undergo further (secondary) peeling. Beyond backbone degradation, substituent reactions are also significant. For instance, the conversion of MeGlcA to hexenuronic acid impacts pulp quality and optical stability. Furthermore, the extensive deacetylation of hemicelluloses results in significant alkali consumption during the initial phase of delignification [60].

3.1.2 Transport of cooking chemicals and lignin

Cooking chemicals

In saturated wood chips, the transport of small ions mainly occur via diffusion, which has been extensively studied [62]. The diffusion rate, commonly characterised by the effective diffusivity D_{eff}, varies substantially depending on several factors, including process conditions (e.g. temperature and pH) and the heterogeneous nature of wood (anisotropic structure, species-related variations, etc.). Consequently, reported values of effective diffusivity likewise differ depending on the conditions under which they were determined.

McKibbins presented one of the earliest studies on diffusion in wood, investigating the release of sodium ions from kraft-pulped chips under neutral conditions [63]. The resulting diffusivities were on the order of $5 \times 10^{-10}\,\mathrm{m^2\,s^{-1}}$ in the longitudinal direction and approximately half this value in the transverse direction. Comparable longitudinal diffusivities have been reported for untreated wood; however, tangential diffusivities were found to be approximately forty times lower [64]. This discrepancy is likely attributable to the partial delignification of the cell walls in the pulped chips studied by McKibbins, which generates additional porosity as material is removed from the lignocellulosic matrix [65]. Tangential transport is therefore enhanced during delignification, as it partly occurs through the cell walls, whereas longitudinal transport remains relatively unchanged, being primarily governed by transport along the lumina.

This behaviour is consistent with observations by Talton and Cornell, who reported that radial diffusivity increased by a factor of three when transitioning from untreated wood to pulp corresponding to a yield of 65% [66]. In addition, the directional dependence of diffusivity is influenced by fibre swelling induced by increasing alkalinity. Estimates of the effective capillary cross-sectional area (ECCSA) suggested that the ratio between longitudinal and radial transport decreased from approximately 5 to about 1 as the pH increased from 9 to 14 (c.f Figure 3.3) [67].

Transport within the fibre wall, in contrast, has been investigated to a much lesser extent. By tracing the diffusion of tritiated water in small wood particles, it has been shown that the apparent diffusivity decreases with decreasing particle size [68]. This behaviour is consistent with the expectation that, as particle size is reduced, transport increasingly reflects diffusion within the cell wall itself, owing to the diminished contribution from connectivity through lumina. These findings therefore indicate that diffusion within the cell wall is more restricted than transport in intact wood chips.

In addition, it remains unclear whether diffusion within the cell wall proceeds through the rubbery amorphous lignocellulosic network itself or via aqueous micro- and nanopores embedded within this matrix [69]. Attempts to estimate cell wall diffusivity using copper ions reported values several orders of magnitude lower than those associated with water transport in wood [70]. An alternative

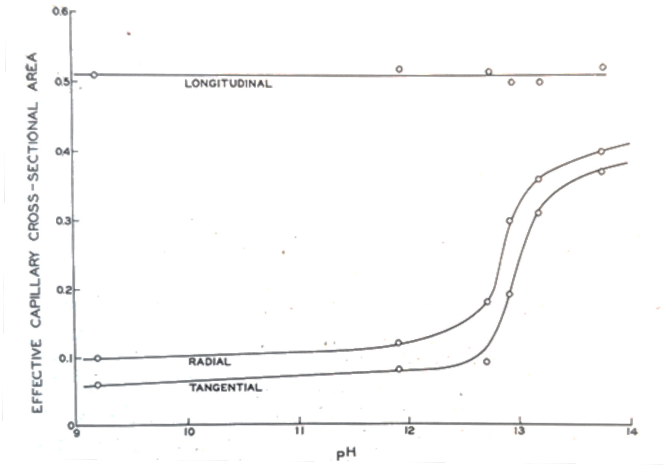

Figure 3.3: Directional dependence of the effective capillary cross-sectional area (ECCSA) after soaking for 24hr at different pH levels, as measured by Stone [67]. Reprinted with permission.

approach have involved diffusion experiments using cellulose membranes with pore sizes comparable to the interfibrillar spacing in the cell wall, yielding diffusivities on the order of $10^{-11}\,\mathrm{m^2\,s^{-1}}$ [71].

Lignin

The diffusion of dissolved wood components, and lignin in particular, remains poorly understood, with only a limited body of literature addressing lignin-specific diffusivity estimates. The free diffusivity of lignin in solution has been reported to be on the order of $10^{-10}\,\mathrm{m^2\,s^{-1}}$ in 1 M NaOH [72], whereas values approximately one order of magnitude lower have been estimated under neutral conditions [36]. During diffusion within wood chips, transport is expected to be more hindered, corresponding to lower effective diffusivities. At the same time, elevated temperatures during cooking may partially offset this restriction. Consistent with this, reported diffusivities for lignin in wood chips under cooking conditions are also on the order of $10^{-10}\,\mathrm{m^2\,s^{-1}}$ [9, 73]. In contrast, substantially lower diffusivities have been reported for ambient treatments in alternative processes, such as acetic acid fractionation of sugar bagasse, where values in the range 10^{-14}–$10^{-12}\,\mathrm{m^2\,s^{-1}}$ were obtained [74]. Even lower values, down to $4 \times 10^{-19}\,\mathrm{m^2\,s^{-1}}$, have been reported for organosolv treatment of cedar [75].

As observed for small ions, diffusion of lignin within the fibre cell wall is considerably more restricted. Estimates based on leaching experiments of kraft pulps at neutral and ambient conditions suggest a cell wall diffusivity on the order of $10^{-17}\,\mathrm{m^2\,s^{-1}}$ [76]. Li et al. reported pronounced pH dependence, with a bimodal distribution of diffusivities ranging from 10^{-17} to $10^{-13}\,\mathrm{m^2\,s^{-1}}$ at pH 14, as illustrated in Figure 3.4 [77]. Similarly, Pahlevanzadeh and van Heiningen estimated diffusivities in the range 10^{-17}–$10^{-15}\,\mathrm{m^2\,s^{-1}}$ during alkaline leaching at intermediate temperatures in the context of oxygen delignification [78]. Con-

siderably higher values, on the order of 10^{-13}–$10^{-12}\,m^2\,s^{-1}$, have nonetheless been reported based on diffusion experiments through cellulose membranes, as discussed previously [79]. However, as highlighted by Li *et al.*, diffusivities depend in part on lignin size, which may help explain discrepancies among the studies. For example, the residual pulp lignin released in the leaching experiments is expected to contain larger molecular fractions than the technical kraft lignin employed in the study using cellulose membranes.

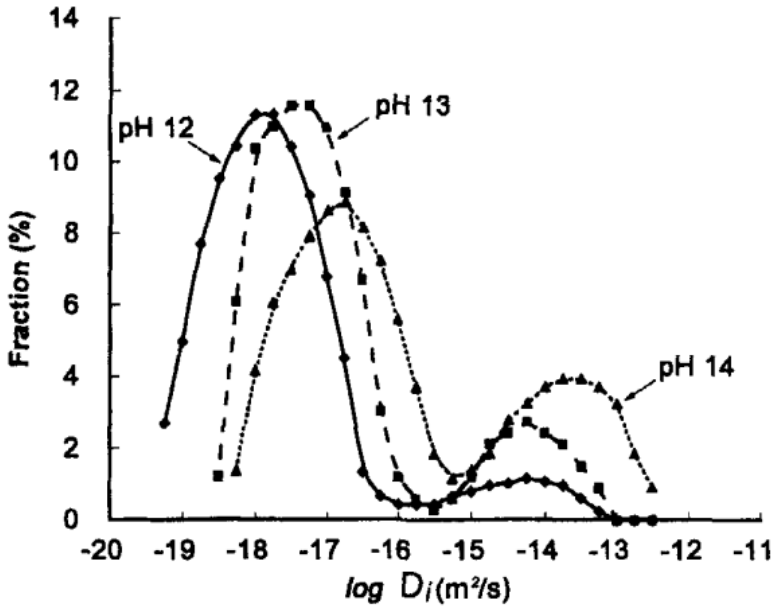

Figure 3.4: Bimodal distribution of lignin diffusivities, as estimated from the pulp leaching experiments by Li *et al.* [77]. Reprinted with permission.

3.1.3 Lignin solubility

As discussed in Section 3.1.1, the primary objective of lignin-cleaving reactions during pulping is to render lignin soluble. Only in its solubilised form can lignin be transported out of the wood matrix, thereby enabling fibre separation prior to subsequent papermaking operations. Owing to the inherent recalcitrance of lignin, however, solubility remains limited unless the polymer is extensively degraded or chemically modified. Even under kraft pulping conditions, a fraction of the dissolved lignin is close to its solubility limit [80]. As a consequence, lignin may re-adsorb onto fibre surfaces, particularly towards the end of pulping, when lignin concentrations are high and the effective alkali concentration is reduced [81]. Factors governing lignin solubility are therefore of critical importance in kraft pulping. Nevertheless, the wide variability in lignin properties arising from differences in origin and isolation method necessitates that such effects are discussed only in general terms [17].

One of the key determinants of lignin solubility in aqueous media is the abundance and distribution of hydroxyl functional groups, which impart polarity

upon dissociation at elevated alkalinity. Two classes of hydroxyl groups are commonly identified as the main contributors to lignin solubility: carboxylic acids and phenolic hydroxyl groups [82]. Carboxylic acids are readily dissociated at alkaline conditions, but do not occur to any substantial extent on the lignin backbone itself. However, they are present on carbohydrates which are covalently linked to lignin through so-called lignin carbohydrate complexes (LCCs), which has led to the suggestion that these components co-dissolve with lignin fragments [61, 83]. Phenolic hydroxyl groups, in contrast, are directly bound to the aromatic backbone of lignin and have been shown to correlate strongly with increased solubility [84]. Their pK_a values, typically in the range 9.5–10.5, correspond closely to the pronounced changes in precipitation yield observed around these pH levels [85]. In addition to functional group chemistry, lignin solubility is strongly influenced by molecular weight [84–87]. It has been debated, however, whether solubility is primarily governed by absolute molecular size or by the relative abundance of solvation-promoting functional groups [88]. A further, well-documented factor affecting lignin solubility is its interaction with cationic species [82], the effects of which vary substantially among ions of both equal and different valencies [89].

3.2 Delignification kinetics

Substantial effort has been devoted to elucidating the kinetics of pulping, with particular emphasis on the main delignification reactions occurring during the cooking stage. Despite this, no clear consensus has been reached regarding the relative importance of the individual steps outlined in Section 3.1. Although these steps occur concurrently at a general level, they are fundamentally sequential and all are required for complete delignification. The overall rate is therefore expected to be controlled by the slowest of these processes. As a result, to reduce the complexity associated with describing the full delignification mechanism, many kinetic descriptions and models reduce the complexity of the full delignification mechanism by focusing on one, or a limited subset, of the steps that are assumed to control the overall delignification rate.

3.2.1 Experimental rate studies: Reactions

The role of OH^- and HS^-

Historically, the delignification has frequently been approximated as a pseudo-homogeneous process, with cleavage of the aryl–ether β-O-4 linkage regarded as the rate-limiting step [55]. On this basis, considerable attention has been directed towards understanding how the concentrations of the active kraft cooking chemicals, OH^- and HS^-, influence the reaction kinetics. Early studies employing lignin model compounds reported that the rate of cleavage of non-phenolic β-O-4 linkages scales linearly with the OH^- concentration [90, 91]. In contrast, phenolic β-O-4 linkages were found to be cleaved rapidly and to exhibit little dependence on the concentrations of OH^- and HS^-, provided that a sufficient minimum level was present. While these investigations provide

valuable insight into the intrinsic chemistry of aryl–ether bond scission, they are based on a limited experimental scope. Moreover, the extent to which kinetic parameters derived from model-compound studies can be transferred to describe delignification kinetics in real wood systems is likely limited [92].

A larger body of work has therefore focused on the kinetics of kraft pulping in intact wood, where delignification is analysed from the perspective of overall reaction behaviour. In these studies, the influence of alkalinity has again been a central theme. However, such investigations reflect only *apparent* reaction kinetics, since observed rates inherently include contributions from e.g. transport phenomena and evolving wood structure. As a result, the apparent dependencies on OH^- and HS^- vary substantially throughout the course of the cook.

The initial phase of delignification, commonly associated with the cleavage of phenolic aryl–ether bonds, has been reported to proceed rapidly and to be essentially independent of alkali concentration within the investigated range [93]. Based on these observations, it has been suggested that early delignification may instead be limited by alkali transport rather than by reaction kinetics. The subsequent stage, during which the majority of lignin is removed, has traditionally been attributed to cleavage of non-phenolic β-O-4 linkages [55]. Kinetic studies indicate that this stage depends on the OH^- concentration and also exhibits a weaker, but significant, dependence on HS^- [11, 52, 94, 95]. Furthermore, an increased HS^- concentration during the impregnation or pre-treatment stage has been shown to reduce the apparent HS^- dependence observed during bulk delignification [95], indicating that sulphide concentration influences reactions occurring at earlier stages of the process as well. The final phase of delignification is commonly associated with the slow cleavage of carbon–carbon linkages, for example through retro-aldol reactions [55]. This stage has been reported to show a weaker dependence on OH^- concentration and to be largely independent of HS^- [96, 97].

Although observations of apparent pulping behaviour are of practical relevance, their utility for elucidating the underlying mechanisms of delignification is limited. This has led to inconsistencies when attempting to assign observed kinetic features to specific chemical or transport phenomena. For example, the reported independence of alkali concentration during early delignification cannot be fully explained by diffusion limitations alone, since alkaline transport itself depends on OH^- concentration. Similarly, HS^- concentration evidently influences large portions of the delignification process, despite being associated primarily with reactions occurring at the very beginning of the cook [55]. Taken together, these observations suggest that kraft delignification cannot be adequately described as a simple pseudo-homogeneous reaction system, as its kinetic behaviour reflects the interplay of many contributing factors.

Lignin composition

Variations in lignin composition have long been proposed to influence delignification behaviour in hardwoods, with particular emphasis placed on the ratio between syringyl and guaiacyl units, commonly expressed as the *S/G ratio*. Numerous studies have reported that higher S/G ratios are associated with faster delignification and improved pulping performance [98–100]. Despite the apparent consistency of these observations, the mechanisms underlying this relationship remain unresolved, and contrasting interpretations have been proposed.

One explanation focuses on intrinsic differences in bond reactivity. Model-compound investigations have suggested that β-O-4 linkages associated with syringyl units are more readily cleaved than those involving guaiacyl units. It remains unclear whether the observed reactivity differences arise when syringyls constitute the main C_9-units in the β-O-4 linkages [101, 102] or as the ether-linked leaving units in the cleavage reactions [102, 103]. Nevertheless, because such model studies rely predominantly on lignin dimers, their ability to represent the behaviour of the highly cross-linked and carbohydrate-associated lignin network present in wood is likely limited.

An alternative interpretation attributes differences in delignification rates to structural constraints imposed by condensed carbon–carbon linkages. Guaiacyl units possess an available C5 position that promotes the formation of condensed structures, which have been proposed to retard delignification kinetics [104]. From this perspective, the reduced abundance of condensed linkages in syringyl-rich lignin would be consistent with the higher pulp yields reported at elevated S/G ratios [104–106]. However, this structural argument is not universally supported. Several investigations have found little or no correlation between S/G ratio and the yield [107–109].

The apparent importance of S/G ratio may also be influenced by species selection. Much of the available literature is based on eucalyptus species, particularly *Eucalyptus globulus*, which combine high S/G ratios with rapid delignification. The resulting correlations may therefore reflect species-specific behaviour rather than a general dependence on lignin monomer composition. Other hardwoods, such as birch, do not consistently follow the same trends [43, 110]. Consequently, factors beyond lignin composition, including interactions with non-process elements such as calcium, may contribute to the favourable pulping characteristics observed for certain species [111].

3.2.2 Experimental rate studies: Transport of cooking chemicals and lignin

Transport phenomena in kraft pulping have received attention primarily in the context of delivery of cooking chemicals prior to the onset of chemical reactions. In particular, the effects of chip impregnation [112–114] and chip thickness [115–118] have been widely investigated. These studies largely address the

penetration of reactive species (i.e hydroxide and hydrosulphide ions), from the bulk liquor into the chip interior and towards lignin located within the cell wall. In contrast, considerably less attention has been directed towards the subsequent dissolution and transport of fragmented wood components formed during delignification.

Nevertheless, several investigations have reported the existence of distinct concentration levels of dissolved wood components between the liquor contained within wood chips and the surrounding bulk liquor [8–10, 13]. Although the reported magnitude of these differences varies among studies, the consistent observation of chemically distinct liquor fractions implies that mass transfer between them influences the overall rate of delignification. Such transport is governed by factors similar to those affecting the impregnation with small ions, including chip geometry and anatomical features such as vessels, but involves substantially larger and more chemically heterogeneous species. In addition, the internal morphology of the chip evolves as delignification proceeds, leading to time-dependent changes in transport pathways and resistances [119].

Beyond the chip scale, transport limitations have also been suggested to affect the fibre cell wall level (corresponding to item 6 in Section 3.1) [8, 12]. Mass transfer within the cell wall is inherently complex due to its heterogeneous structure and the diverse chemical nature of dissolved lignin fragments. Both the composition of the cell wall and the properties of the dissolved species evolve continuously throughout the cook, in parallel with changes in alkalinity. As a result, experimental studies directly addressing transport kinetics within the cell wall remain scarce, and most available evidence is indirect. Existing observations suggest that transport may depend on cell wall thickness [11] as well as steric and electrostatic interactions between dissolved lignin fragments and the fibre wall matrix [77, 120]. However, direct experimental characterisation of lignin transport kinetics within the fibre wall under kraft pulping conditions has not yet been reported.

3.2.3 Experimental rate studies: Lignin solubility

It has been suggested that mechanisms limiting lignin solubility become increasingly important during the later stages of delignification [121]. Although the kinetics of lignin dissolution itself have been modelled as relatively rapid [122], solubility constraints may nevertheless influence the overall rate of delignification indirectly. One prominent example is the effect of cation concentration in the cooking liquor, commonly referred to as the ionic strength (IS), which has been consistently reported to correlate with the delignification rate [52, 97, 123]. This behaviour is commonly attributed to reduced lignin solubility at elevated IS levels. However, alternative explanations have also been proposed, including the influence of ion-exchange and electrostatic partitioning phenomena described by Donnan theory, which may affect both reaction environments and mass transport within the fibre wall [80, 120, 124, 125]. Moreover, the molecular weight of dissolved lignins increases continuously during kraft cooking

[10, 126, 127]; however, relatively little is known about the way in which this influences the delignification kinetics.

3.2.4 Numerical modelling

One of the earliest and most influential approaches to modelling delignification kinetics is the *H-factor*, developed by Vroom [128]. This simplified formulation—initially developed for soda conditions—employs an Arrhenius-type expression to combine the effects of time and temperature into a single variable, which can be correlated with the extent of delignification. Hatton later extended this concept by deriving expressions for pulp yield and kappa number based on the H-factor and the effective alkali concentration [129]. However, the model relied on a single rate expression to describe the entire cook, despite well-established changes in alkali consumption and in the relationship between yield and lignin content as delignification proceeds.

Subsequent modelling efforts addressed these limitations by introducing distinct *phases* of delignification [115, 130]. In the model proposed by Teder and Olm, lignin was assumed to react through three sequential phases: the initial, bulk, and residual phases. Each phase was characterised by a different dependence on temperature and on the concentrations of OH^- and SH^-. As noted by the authors, however, changes in chemical concentrations during an early phase, while not influencing the rate of that phase directly, affect the rates of subsequent phases. For instance, although the initial-phase delignification rate was modelled as independent of OH^- and SH^- concentrations, variations in these concentrations during the early stages of the cook influence the final residual lignin content.

A related but more comprehensive framework is the Gustafson model, which has subsequently been widely applied and further developed [131]. This model also describes delignification as a sequence of three phases, but additionally links carbohydrate degradation rates to the delignification rate in each phase. It further incorporates the diffusion of OH^- into the wood chips. Later studies adopted similar kinetic expressions while allowing the delignification phases to proceed in parallel rather than strictly in series [96, 132]. An alternative modelling strategy is represented by the Purdue model, originally developed by Smith [133]. Instead of phase-based kinetics, this approach assumes five distinct reacting components: fast- and slow-reacting lignin, cellulose, glucomannans, and xylans.

Many later models are based on either the Gustafson or the Purdue framework, or on combinations of the two [97, 134–138]. A common modification is the further subdivision of reacting species into smaller subgroups, or the explicit inclusion of non-reactive components [139]. Across these models, lignin is generally represented by empirically defined “fast” and “slow” reacting species or phases. This approach reproduces observed delignification rates but does not explicitly reflect the underlying chemical mechanisms, although some stud-

ies have introduced more detailed reaction expressions intended to represent specific reactions [140, 141].

Despite these refinements, most kinetic models do not explicitly account for the heterogeneity of wood delignification. With a few exceptions [96, 122, 138], they have been developed using experimental data obtained from whole wood chips. Consequently, the estimated kinetics represent *apparent* reaction rates that conflate *intrinsic* chemical reactions with the solubilisation and transport of dissolved components within the chip structure. Although the original model by Gustafson did include diffusion of OH^-, it neglected the transport of other components, and later studies have predominantly assumed homogeneous OH^- concentration profiles as well.

More recently, several models have attempted to address aspects of this heterogeneity. Grénman *et al.* presented a three-dimensional model that incorporates direction-dependent, but otherwise homogeneous, diffusion in wood chips, together with the effects of spatial variations in porosity [15]. Simão *et al.* applied film theory to estimate the influence of external and internal mass-transfer resistances, although concentration gradients were represented using simplified polynomial expressions and only one spatial direction was considered [9]. Gilbert *et al.* introduced a three-phase description in which the heterogeneity of wood chips was represented by distinguishing between solid fibres and the entrapped liquor within the lumen network [13]. Finally, Bijok *et al.* combined several of these approaches to describe interactions between fibres and bound and free liquors in an anisotropic system. Nevertheless, none of these models account for the large disparity between the diffusion rates of dissolved lignin and smaller ions (as discussed in Section 3.1.2). Furthermore, although the model by Bijok *et al.* uses averaged behaviour to represent fibre-level phenomena, these approaches do not resolve the multi-scale heterogeneity inherent to wood.

Chapter 4

Material & Methods

This chapter outlines the materials, instrumentation, and process conditions used in the pulping experiments. Additionally, it details the analytical methodologies employed for the characterization of the raw feedstock, obtained pulp, and process liquors. Finally, a brief overview of the numerical models developed in this work and the numerical procedures used to solve them is included.

4.1 Wood feedstock

The raw feedstock utilized in this work was procured from a Swedish pulp mill, using trees harvested in southern Sweden. Paper I utilized wood derived from individual logs of birch (*Betula pubescens*[1]), beech (*Fagus sylvatica*), aspen (*Populus tremula*), and alder (*Alnus glutinosa*). The birch log also served as the raw material for Paper II and Paper IV. In these studies, the wood was chipped and subsequently cut in a knife mill to particles passing through a 1 mm mesh; this fraction is hereafter referred to as wood meal.

In contrast, Paper III employed a supply of industrially chipped (2–6 mm thick), mixed birch (*Betula pendula* and *Betula pubescens*) . Lastly, in Paper V, the developed model was evaluated against experimental data generated by Marion de Godoy *et al.* [148], utilizing hand-cut chips (about 8 mm thick) originating from the same birch log used in Paper I .

4.2 Kraft pulping

Kraft delignification was experimentally simulated with laboratory scale reactor setups, using a flow-through packed-bed reactor (for wood meal), or autoclave batch reactors (for wood chips). This section briefly details the employed

[1]Differentiation between *Betula pendula* and *Betula pubescens* is generally not prioritized in pulping studies [142–146]. The birch log employed in Paper I was tentatively identified following the protocol described by Lundgren *et al.* [147], although prolonged storage prior to analysis may have influenced the taxonomic determination.

reactor setups and conditions. The full details are included in the appended papers.

4.2.1 Reactor setups

Flow-through experiments were conducted using an established continuous-flow tube reactor system [123, 149, 150], illustrated schematically in Figure 4.1. In each trial, approximately 4 g of wood meal was uniformly packed into the reactor vessel and impregnated at ambient temperature with roughly 30 ml of cooking liquor. To initiate the reaction, the reactor assembly was submerged into a pre-heated polyethylene glycol (PEG) bath maintained at the target temperature. The treatment duration ranged from 5 to 180 minutes, after which the reaction was quenched by immediate immersion in a cold water bath. Following the cook, the resulting pulp was suspended in water, defibrillated using a handheld blender, washed to neutrality, and subsequently dried. The transient temperature experiments was managed by rapidly transferring the reactor setup between two distinct PEG baths preset to the required temperatures.

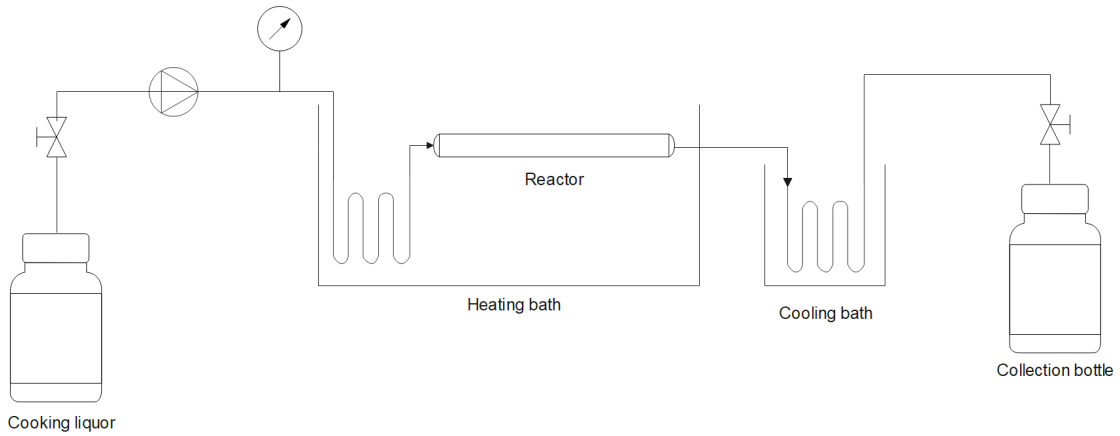

Figure 4.1: Schematic representation of the flow-through reactor setup.

A continuous supply of fresh cooking liquor was drawn from a reservoir at ambient temperature. Prior to entering the reactor, the feed stream was pre-heated by passing through a coiled extension of the feed line submerged within the PEG bath. To maintain a near-constant alkali concentration throughout the process, the volumetric flow rate was modulated; it was increased stepwise to 10 ml/min during the impregnation phase and subsequently reduced to a steady state of 2.5 ml/min from 22 minutes onwards. The transient conditions involving different liquor concentrations were achieved through two reservoirs connected to the reactor inlet by a 3-way valve.

Upon exiting the reactor, the effluent was immediately cooled via a heat exchanger to quench further chemical reactions. The spent cooking liquor (black liquor) was fractionated into discrete samples according to the schedule outlined in Table 4.1, though specific experimental requirements occasionally necessitated deviations from this protocol, as detailed in the appended papers.

Table 4.1: Sampling intervals for black liquor collection

Time interval [min]	Approx. volume [ml]
-5 – 0	30
0 – 5	50
5 – 10	50
10 – 20	90
20 – 40	70
40 – 60	50
60 – 90	80
90 – 120	80
120 – 150	80
150 – 180	80

Batch delignification of wood chips were conducted in 1.5 L stainless steel autoclaves. Each vessel was charged with approximately 25 g of wood chips and chemically treated at a liquor-to-wood (L:W) ratio of 10:1 for Paper III and 22:1 for Paper V. To facilitate impregnation, the autoclaves were initially evacuated for 5–10 minutes, followed by pressurization with nitrogen gas at 5 bar for a duration of 15–20 minutes. In the specific case of Paper III, the spent impregnation fluid was drained and replaced with fresh cooking liquor at an L:W ratio of 20:1 prior to the cook. The trials were initiated by submerging the autoclaves in a preheated PEG bath for defined intervals ranging from 10 to 120 minutes. Autoclaves reached terminal temperature in approximately 25 min, as estimated from the data of Bogren *et al.* [52]. At the conclusion of the specified time, the reactions were quenched by immersion of the vessels in a cold water bath.

For Paper III, the free liquid phase was separated via filtration and designated as bulk liquor (BL). The remaining wet pulp was subsequently centrifuged to isolate the liquor fraction retained within the fiber matrix, referred to as centrifuged liquor (CL). The solid residue was then washed, leached with water until a neutral pH was achieved, and dried. The experimental protocol for Paper V focused exclusively on the solid phase, utilizing a washing and drying procedure analogous to that of Paper III.

4.2.2 Pulping conditions

Throughout this work various pulping conditions have been investigated, as summarized in Table 4.2. The cooking liquor was prepared fresh prior to each cook, and the concentration verified through the ABC-titration, according to

the SCAN N-2 standard.

Table 4.2: Composition of the cooking liquor used in this work.

	Temperature [°C]	Time [min]	OH^- [mol/kg liquor]	HS^- [mol/kg liquor]
Paper I	140, 150	0–180	0.35	0.15
Paper II	150	0–180	0.35	0–0.35
Paper III	160	0–120	0.60	0.15
Paper IV	140, 150, 160	0–180	0.35, 0.70	0.15
Paper V	165	0–60	0.55	0.25

4.3 Characterisation

4.3.1 Compositional analysis

The lignin and carbohydrate compositions of the pulp and liquor fractions were determined using a modified version of the standard analytical protocols established by NREL[151]. Following acid hydrolysis, lignin was quantified as two distinct fractions: acid-insoluble lignin (Klason lignin) and acid-soluble lignin (ASL), the latter of which comprises solubilized lignin fragments, extractives, and reaction byproducts [152]. The resulting soluble hydrolysate was analyzed for carbohydrate monomers via high-performance anion exchange chromatography with pulsed amperometric detection (HPAEC-PAD). All carbohydrate data are reported in their anhydrous forms [153] and have been corrected for hydrolytic degradation losses according to previously established factors [154].

4.3.2 Lignin precipitation

Prior to structural characterisation, the solubilized lignin was recovered from the liquor fractions via precipitation, following the protocol outlined by Dang *et al.* [127]. Briefly, the liquor samples were acidified to pH 2.5 using sulphuric acid, subjected to freezing overnight, and subsequently thawed. The precipitate was recovered via filtration, washed with acidified water (pH 2.5) to eliminate soluble impurities, and dried at 40°C for 3 days. The isolated material, designated as *precipitated lignin*, contained varying proportions of co-precipitated carbohydrates. To preserve the structural integrity of these associated carbohydrate moieties and prevent the loss of any lignin fractions, no further purification steps were undertaken.

4.3.3 Molecular weight distribution

The molecular weight distributions (MWD) of the precipitated lignin fractions were determined using gel permeation chromatography (GPC) on a PL-GPC 50

Plus system (Varian Inc.). Chromatographic separation was performed using two PolarGel-M columns (300 × 7.5 mm) with a mobile phase of dimethyl sulfoxide (DMSO) containing 10 mM LiBr, delivered at a flow rate of 0.5 ml/min. Prior to analysis, the lignin samples were dissolved in the eluent overnight and subsequently diluted to a concentration range of 0.25–2.0 mg/ml. Detection was achieved using ultraviolet (UV) and refractive index (RI) detectors connected in series. The system was calibrated using pullulan standards covering a molecular weight range of 0.18–708 kDa.

4.3.4 Nuclear Magnetic Resonance spectroscopy

Structural characterization of the precipitated lignin fractions was performed using 2D heteronuclear single quantum coherence (HSQC) NMR spectroscopy. Spectra were acquired using the standard pulse sequence *hsqcedetgpsisp2.3*, utilizing 24 scans and a 1 s relaxation delay. The data matrices consisted of 3072 and 512 points for the ^{1}H and ^{13}C dimensions, respectively. Instrumentation varied by study: a 700 MHz spectrometer was utilized for Paper I, while Paper II and Paper III employed an 800 MHz system, both of which Bruker Avance III systems. Prior to analysis, lignin samples were dissolved in DMSO-d_6 at a concentration of 140 mg/ml overnight. To eliminate minor insoluble fractions (<5 wt%), the solutions were centrifuged at 12,500 rpm for 5 minutes.

4.4 Numerical modelling

Two delignification models were developed as part of this work: an initial model describing delignification within the cell wall, and a subsequent extension that incorporates wood-chip-level transport. The principal steps of the model development and validation are summarised in Sections 5.3 and 5.4, with detailed descriptions provided in Paper IV and Paper V, respectively.

The cell-wall model describes one-dimensional transport and reaction along the radial direction of a simulated fibre wall, without distinguishing between the cell wall and the middle lamella. One boundary represents the symmetry plane between adjacent fibre walls, while the opposite boundary corresponds to the interphase with the lumen. The wood-chip model employs a multi-scale framework: the cell-wall domain is treated in the same manner as in the initial model, while an additional domain accounts for the one-dimensional transport of OH^- along the radial direction at the chip scale. For simplicity, both models use normalised spatial coordinates, with the cell-wall thickness defining the length scale at the cell-wall level and the chip thickness defining the length scale at the chip level.

The lignin concentration was also normalised. In the cell-wall model, the concentration was normalised against the measured lignin content of the wood after impregnation at room temperature. This choice was motivated by the observation that a portion of the lignin (approximately 11% of the initial amount)

was already removed under these mild conditions. This early removal—likely dissolution—mechanistically differs from the reaction and mass transport that governs the main delignification process, as the latter becomes relevant only at significantly elevated temperatures. Because the model was intended to describe delignification under industrially relevant, high-temperature conditions, it only included these latter mechanisms. It would therefore not be expected to reproduce the initial dissolution observed at room temperature.

An improved normalisation approach was introduced in the wood-chip model. Here, the data were instead normalised against the lignin content of untreated wood, although the initial conditions were adjusted such that the normalised lignin content at time zero corresponded to the measured level in the impregnated wood. This procedure avoids the bias introduced by the previous normalisation scheme, although its effect on the overall model results was relatively minor (cf. Table 5.2).

The equations associated with each model were solved using MATLAB's *pdepe* solver, and the fitting of parameters for the cell wall model was achieved using the *lsqnonlin* tool. For the cell-wall model, a spatial resolution of 14 nodes—unevenly distributed to provide a finer grid near the lumen boundary, where large gradients were expected—was found to be sufficient. The temporal resolution was controlled automatically by the *ode15s* solver embedded within the *pdepe* framework.

The wood-chip model required a finer spatial discretisation to ensure convergence. A total of 30 nodes were used for the cell-wall dimension, whereas 70 nodes were required for the chip-level domain. During model development, the temporal progression of the chip-level simulation also required explicit control; for most conditions, a maximum time-step of 0.1 s was necessary to obtain converged solutions. The cell-wall domain was solved at each chip-level time step, with its temporal resolution again controlled automatically by the solver.

Chapter 5

Results & Discussion

This chapter presents a summary of the main findings from the five appended papers. It begins with an overview of the delignification behaviour of birch wood meal with respect to time, temperature, and cooking liquor composition, followed by an analysis of the resulting dissolved lignin. Differences in delignification kinetics among the investigated hardwoods are then briefly summarised, after which the delignification of birch wood chips is examined. Finally, the heterogeneous cell-wall delignification model is presented together with its subsequent integration into a multi-scale wood-chip model.

5.1 Cell wall delignification

A flow-through reactor was employed for wood meal experiments, offering two primary advantages over conventional batch reactors. First, continuous sampling of the spent black liquor enabled a time-resolved characterization of the dissolved wood components throughout the process, rather than yielding only average properties at the end of the experiment. Second, the combination of short residence time and immediate cooling allowed for the characterization of the components structure as they were released from the wood matrix, thereby minimizing the secondary degradation that typically occurs in batch systems.

5.1.1 Kinetics of birch wood meal delignification

Lignin

Delignification of birch wood meal constituted the basis of Papers I, II, and IV. Figure 5.1 illustrates the decrease in lignin content of the wood tissue over time at different temperatures. Notably, the divergence between temperature conditions increased initially, reaching a maximum at the 60 min data, after which the differences between conditions diminished. An interpretation of this behaviour is the indication of a strongly temperature-dependent phenomenon governing the early-stage delignification kinetics, whose influence appears to

diminish after roughly an hour. Nevertheless, as the diminishing rates coincide with reduced lignin levels, this behaviour could reflect any phenomenon whose rate is dependent on the residual lignin content, and therefore cannot be attributed to a single mechanism.

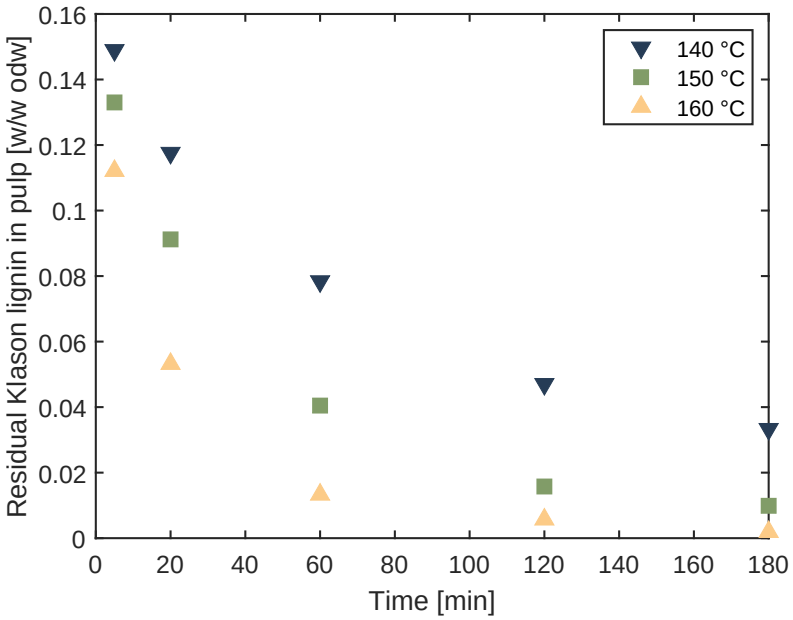

Figure 5.1: Remaining Klason lignin content in birch wood meal after pulping at various temperatures. The OH^- and HS^- concentrations were 0.35 M and 0.15 M, respectively. Values are normalized to the initial wood weight.

The effect of varying HS^- concentration is presented in Figure 5.2, showing that HS^- markedly increased the delignification rate across the analysed range. In addition, data from cooks conducted at elevated OH^- levels are included, indicating that the effect of HS^- was of the same order of magnitude as that of OH^-. The influence of HS^- was further examined under transient conditions, in which the process liquor was switched from regular kraft to soda liquor (containing no HS^-) after different reaction times (Figure 5.3). When this transition occurred early, a pronounced reduction in the extent of delignification was observed. In contrast, switching the liquors after 60 minutes resulted in negligible differences compared to the kraft reference, suggesting that, under the present experimental conditions, HS^- had a minimal impact on the delignification rate beyond this point. Notably, the contribution of phenolic β-O-4 cleavage is expected to diminish significantly earlier in the process, owing to the relatively low abundance and faster reaction rates of these linkages compared to their non-phenolic counterparts [55, 155].

Consequently, these findings suggest that additional sulphide-dependent reactions may influence the overall delignification rate. The sulfidolytic demethylation reaction is a plausible mechanism, and its impact on delignification is corroborated by the MWD data, as elaborated later in this section.

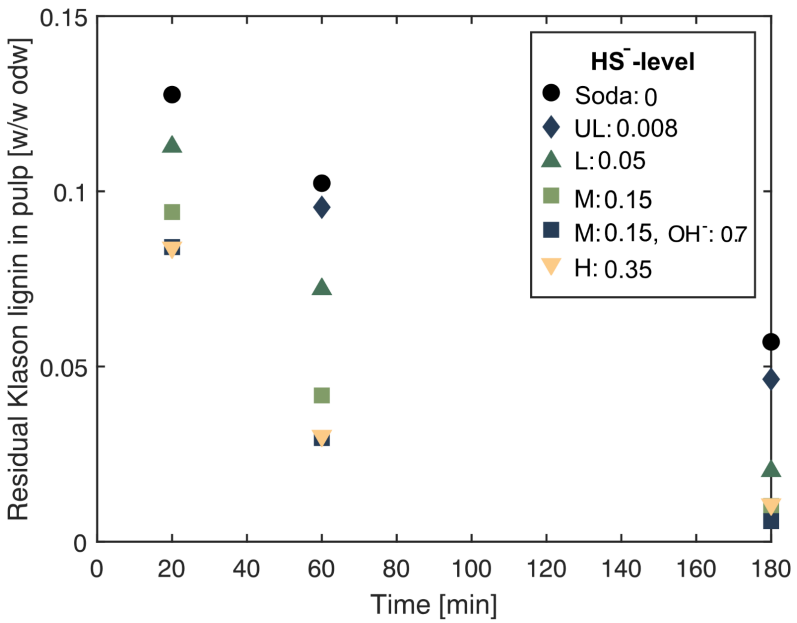

Figure 5.2: Remaining Klason lignin content in birch wood meal after pulping at various times and HS^- levels. The OH^- concentration was maintained at 0.35 M, except where otherwise indicated. Values are normalized to the initial wood weight.

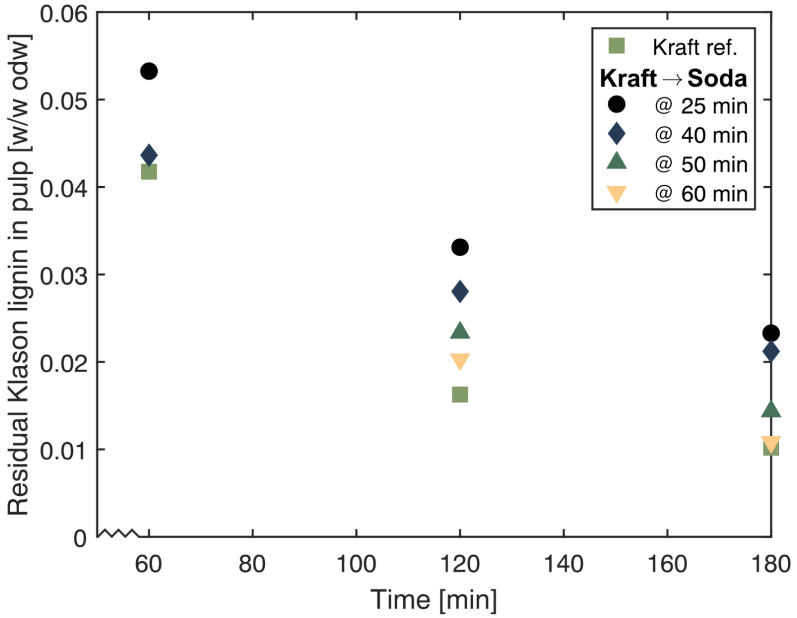

Figure 5.3: Variations in remaining Klason lignin content in the birch wood meal during pulping under transient conditions. The cooking liquor was switched from kraft (HS^-: 0.15 M; OH^-: 0.35 M) to soda (no HS^-; OH^-: 0.35 M) after the time points indicated in the legend. Values are normalized to the initial wood weight.

Xylan

Compared with lignin, xylan removal proceeded much more rapidly, with a substantial portion of the xylan removed within the first 5 minutes (see Figure 5.4). Despite this rapid initial loss, the remaining xylan content in the prolonged experiments appeared to approach a constant value, suggesting the presence of a relatively large fraction resistant to further removal. Notably, the discrepancies between the data obtained at different temperatures appear roughly constant from the first measurement after 5 minutes onward, indicating that any strongly temperature-dependent mechanisms are likely confined to the very early stages of the cook.

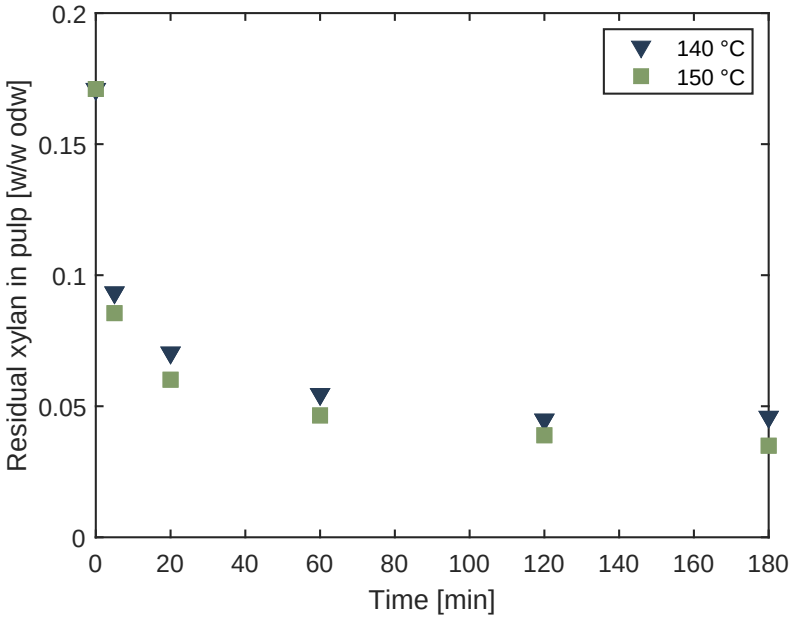

Figure 5.4: Remaining xylan content in birch wood meal after pulping at various times and temperatures. Values are normalized to the initial wood weight.

5.1.2 Size and structure of dissolved wood components during kraft pulping

Lignin

In addition to the compositional analysis of the pulp, the analysis of dissolved lignin was a key factor in elucidating the delignification kinetics. The evolution of the molecular weight distribution of the dissolved lignin is presented in Figure 5.5. Regardless of process temperature, very similar MWD profiles were observed during the first 20–40 minutes. However, from this point onwards, the MWD shifted continuously toward higher molecular weights. As shown in Figure 5.5, the MWD of the dissolved lignin is strongly correlated with the extent of delignification, with a greater proportion of high-molecular-weight fractions eluting from the more extensively delignified pulp of the 150°C experiments. When comparing samples with similar degrees of delignification

(e.g., 120 min at 140 °C vs. 60 min at 150 °C), the profiles are remarkably consistent.

This behaviour can be attributed to transport resistance: larger lignin fragments possess lower mobility than smaller fractions, requiring longer diffusion times—and potentially a more open, less obstructed cell wall matrix—to migrate into the liquor. Consequently, increasingly larger fractions elute as the process progresses.

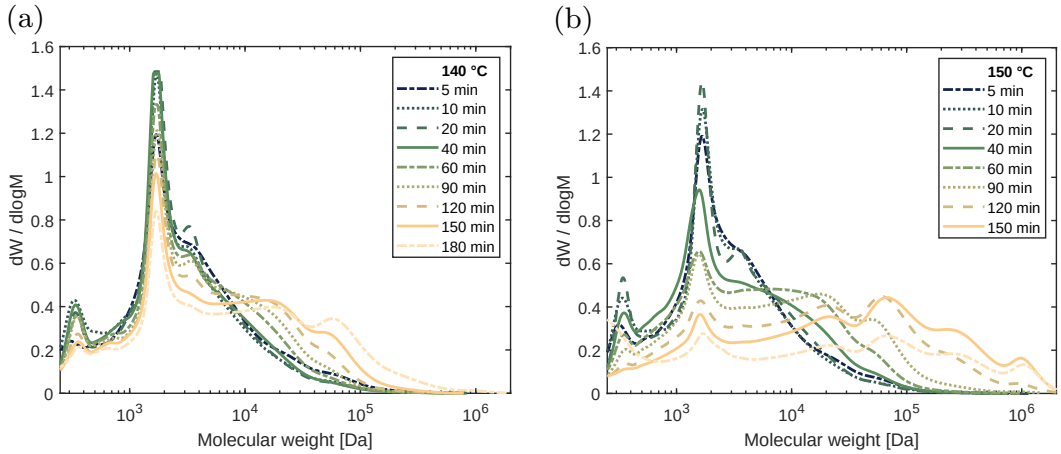

Figure 5.5: Molecular weight distribution of lignin precipitated from black liquor fractions of birch wood meal cooks at (a) 140 °C and (b) 150 °C. Cooking liquor composition: 0.35 M OH^- & 0.15 M HS^-.

The MWD of the dissolved lignin was further investigated during pulping at various HS^- levels. Figure 5.6 depicts the distributions at four different time intervals (a–d) across five distinct levels of sulphidity. Notably, lignin from cooks with no or very low sulphidity exhibited drastically different MWD profiles compared to the kraft treatments. Specifically, the soda lignin displayed a single dominant broad peak with minimal variation throughout the process. In contrast, the kraft lignin MWDs were initially dominated by a distinct peak around 1300 Da—completely absent in the soda lignin—which diminished over time in favour of increasingly higher molecular weight fractions. Consistent with Figure 5.5, the progressive shift of the MWD towards larger fractions is more pronounced at higher degrees of delignification (e.g., at higher HS^- concentrations). This distinction between the soda/ultra-low HS^- and low/medium/high HS^- concentration-regimes parallels the trends observed for the delignification rate (cf. Figure 5.2), further underscoring the interplay between molecular weight and the overall rate of delignification.

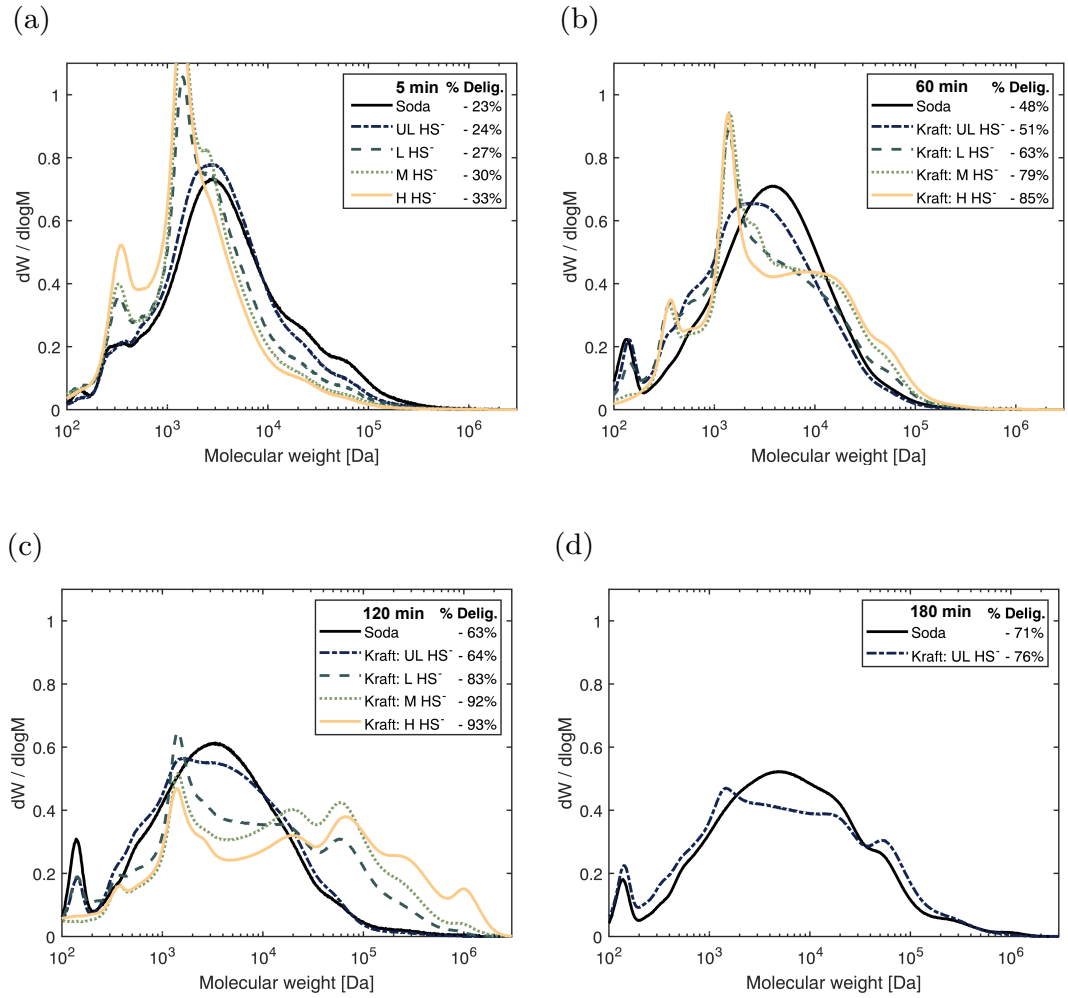

Figure 5.6: Molecular weight distributions of lignin precipitated from black liquor sampled after (a) 5, (b) 60, (c) 120, and (d) 180 minutes during soda and kraft cooking of birch wood meal at constant OH^- (0.35 M) and at ultra-low (UL), low (L), medium (M), and high (H) HS^- concentrations. The legends include the degree of delignification for each sample, which was either measured (b & d) or estimated (a & c) based on the data presented in Figure 5.2.

As previously noted, the trends observed in the transient experiments (Figure 5.3), together with the significant impact of HS^- on the MWD of the dissolved lignin, can likely be attributed to the demethylation reactions known to occur during kraft pulping. Since these reactions are considered relatively slow compared with β-O-4 cleavage [122], this hypothesis aligns well with the behaviour observed in Figure 5.3, where HS^- influenced the delignification rate for a longer duration than would be expected from β-O-4 cleavage alone. The mechanism behind this enhanced delignification likely stems from the introduction of phenolic groups by the demethylation, which promotes lignin solubility [88, 156]. Furthermore, demethylation has been shown to facilitate the extraction of residual lignin, albeit in other contexts than kraft pulping [157].

Demethylation alone, however, is unlikely to explain the distinct peaks around 1300 Da and below that appear exclusively in the kraft samples. Further dis-

tinctions between kraft and soda lignin were revealed by the HSQC NMR data (Figure 5.7). The kraft lignin exhibited several signals that were either absent or significantly diminished in the soda lignin, with similar trends observed in transient cooks transitioning from kraft to soda conditions. These signals were mainly attributed to two types of structures. First, as indicated by the magenta region 1 in Figure 5.7, stilbene structures were identified in the kraft lignin. They are known to form from phenylcoumaran and β-1 linkages following the reverse aldol reaction catalyzed by HS^- or OH^- [32]. The increased abundance in the kraft lignin may thus be explained by the greater nucleophilicity of HS^- compared with OH^-. Since the reactions known to generate stilbenes neither fragment the lignin backbone to any considerable extent, nor introduce structures that promote solubility, they are unlikely to influence the delignification rate.

The second group of signals, observed unique to the kraft spectra, likely corresponds to various condensed structures, suggested to originate from radical-induced repolymerisation reactions involving disulphides [54]. Similar structures have been observed in fractionated lignin, which indicated that these repolymerisation reactions mainly generate relatively low-molecular-weight structures [32, 158]. Such small structures are likely readily removed from the cell wall and are, therefore, not expected to significantly affect the overall delignification rate. It is, therefore, possible that the structures appearing in the 1300 Da range in Figure 5.6 originate from these repolymerisation reactions. This would further explain the significant reduction of the fraction observed around 200 Da in the kraft samples, as this fraction could potentially represent monomeric degradation products that, in the presence of sulphur, form these repolymerised low-molecular-weight structures. Moreover, transient experiments demonstrated that these small structure are rapidly removed upon switching from kraft to soda conditions, indicating little impact on the overall delignification rate (c.f *Figure S1* in the supporting material to Paper II)

It is thus likely that demethylation reactions enable the dissolution of larger lignin molecules; this, in turn, would promote delignification during the final stage of the cook, which is dominated by the removal of these large lignin fractions. Although other sulphide-involving reactions may impact the size and structure of the dissolved lignin, their effect on the overall delignification rate appear limited.

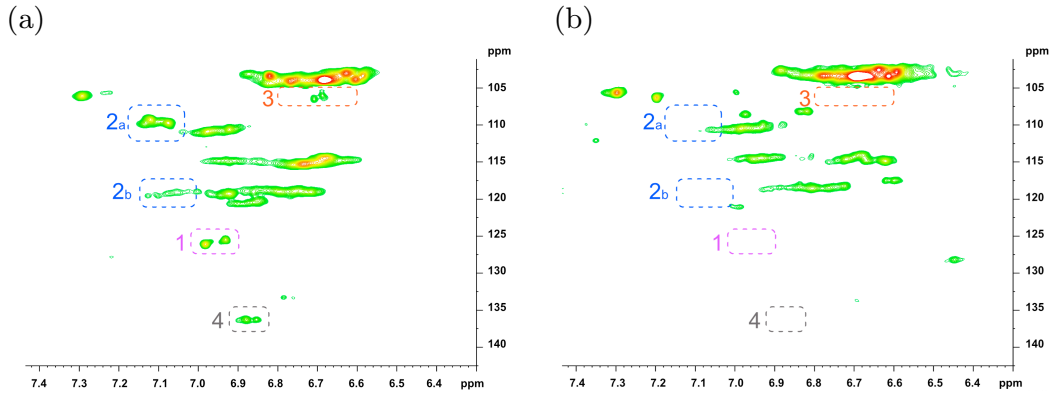

Figure 5.7: HSQC NMR spectra of lignin precipitated from (a) kraft (0.15 M HS^-) and (b) soda cooks of birch wood meal at 150 °C and 0.35 M OH^-. Samples were collected after 5 minutes (kraft) and 20 minutes (soda), corresponding to delignification degrees of 30% and 34%, respectively. Highlighted areas indicate regions with substantially weaker signals in the soda spectrum. Region 4 (grey) remain unidentified.

Xylan

A considerable fraction of carbohydrates (consisting of >97% xylan) co-precipitated with the lignin recovered from the black liquors. A comparison of the UV and RI responses from the SEC data facilitates detection of these carbohydrates, as these structures exhibit negligible UV absorption. This comparison is illustrated in Figure 5.8. As inferred from the appearance of a peak at approximately 20 kDa in the RI trace, these co-precipitated xylans appear to have dissolved primarily as polymers, rather than as degraded mono- and oligomers.

This observation implies that mass transfer limitations may also govern carbohydrate removal. Furthermore, this peak diminishes markedly over the first 10 minutes, a timeframe that coincides with the xylan removal observed in Figure 5.4.

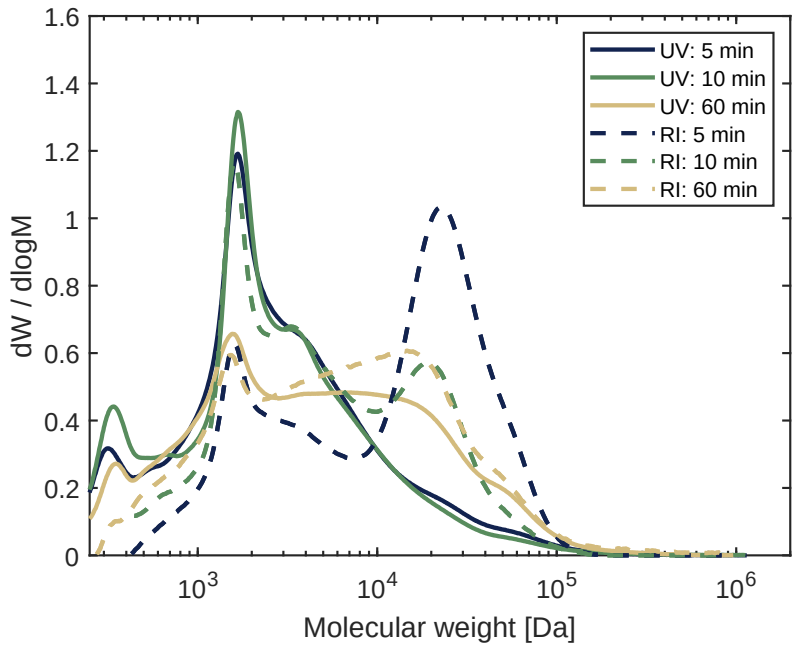

Figure 5.8: Comparison of UV and RI detection data for the molecular weight distribution of lignin and co-precipitated xylan from cooks at 150°C.

5.1.3 Comparison of Nordic hardwoods

The chemical compositions of the birch, beech, aspen, and alder wood investigated in Paper I are summarised in Table 5.1. Overall, birch exhibited a comparatively low lignin content coupled with a high proportion of xylan, whereas aspen was characterised by elevated glucan and mannan contents alongside relatively low levels of xylan and lignin. In contrast, both beech and alder displayed relatively high lignin contents. These compositional profiles align with previously reported data for these species [17, 24, 42, 43, 46, 159–161]. However, direct comparisons across studies should be approached with caution, as variations in analytical and characterisation methods can significantly impact the reported values. Furthermore, certain constituents that may influence delignification behaviour—such as extractives and hemicellulose side groups—were not quantified in the present work.

Table 5.1: Composition of the untreated wood used in Paper I. Reported values are the average of 4 replicates and corresponding standard deviations. [% on odw]

Component	Birch	Beech	Aspen	Alder
Carbohydrates[a]	63.6 ± 0.6	61.1 ± 2.0	65.8 ± 0.4	62.6 ± 0.4
Glucan	39.1 ± 0.4	39.5 ± 1.3	44.8 ± 0.2	41.5 ± 0.2
Xylan	21.9 ± 0.1	19.0 ± 0.6	17.2 ± 0.2	18.1 ± 0.1
Mannan	1.6 ± 0.0	1.4 ± 0.1	2.9 ± 0.0	1.8 ± 0.1
Arabinan	0.3 ± 0.0	0.4 ± 0.0	0.3 ± 0.0	0.3 ± 0.0
Galactan	0.7 ± 0.0	0.8 ± 0.0	0.6 ± 0.0	0.8 ± 0.0
Klason lignin	19.6 ± 0.2	22.4 ± 0.1	19.0 ± 0.2	24.4 ± 0.4
Acid soluble lignin	5.0 ± 0.1	4.4 ± 0.1	4.7 ± 0.1	3.5 ± 0.1
Total	88.2 ± 0.7	87.9 ± 2.0	89.5 ± 0.3	90.5 ± 0.7

[a] Values given in anhydrous form

Wood meals of all four hardwood species were subjected to similar flow-through kraft delignification experiments as previously described; the corresponding rates of lignin and xylan removal are presented in Figure 5.9. The results show modest variations between the species, with differences primarily attributable to the initial chemical composition of each wood type. However, despite its initially low lignin content, aspen displayed a distinctly faster initial delignification rate, whereas alder exhibited somewhat slower kinetics towards the latter stages of the cook. Even less variation was observed in xylan removal (Figure 5.9(b)), although the birch black liquor contained significantly higher quantities of dissolved—and detectable—xylan (see *Figure 3(C)* in Paper I).

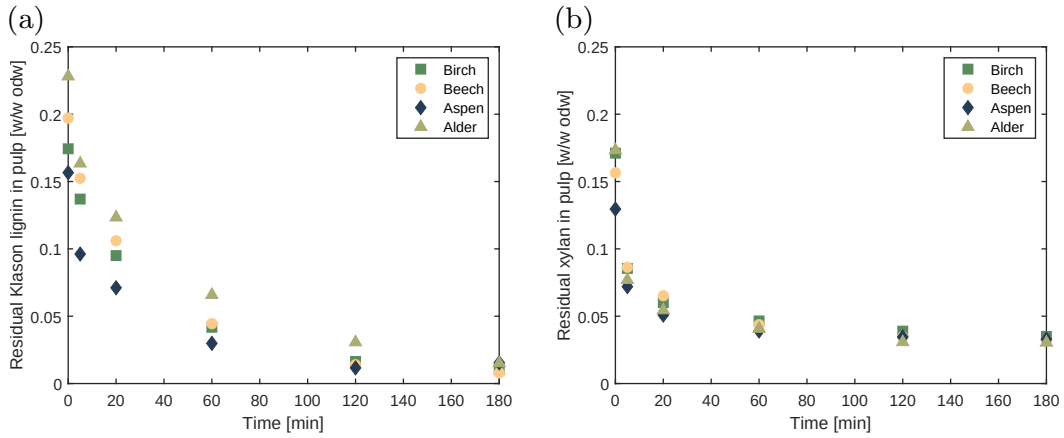

Figure 5.9: (a) Remaining lignin and (b) xylan content in wood meal from alder, aspen, beech, and birch after pulping at 150 °C. Values are normalized to the initial wood weight.

The measured MWD of lignin dissolved from the black liquors of the four species showed no considerable differences (Figure 5.10), indicating that the variations in delignification rate noted in Figure 5.9, although minor, cannot be attributed to the molecular weight of the dissolved lignin. Instead, these variations likely stem from physical characteristics. For instance, the aspen wood meal possessed a noticeably finer texture compared to the other three hardwoods, suggesting a higher specific surface area and potentially greater exposure of the middle lamella. This could account for the accelerated initial delignification observed for aspen. However, it should be noted that observations obtained using a high-magnification digital camera revealed limited morphological variation among the wood meal particles across the four species (see Supplementary Figure S.1 of Paper III).

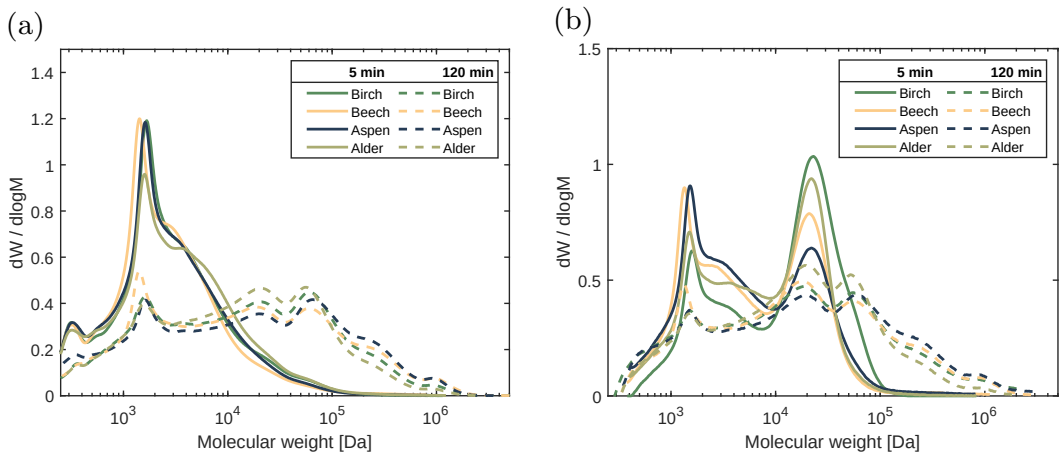

Figure 5.10: Molecular weight distribution of material precipitated from the 5- and 120-minute fractions of all four species during pulping at 150 °C, as detected by (a) UV and (b) RI.

5.2 Wood chip delignification

Part of the experimental work in this thesis was conducted on birch wood chips, as presented in Paper III. The primary objective of that study was initially to investigate the influence of impregnation liquor composition on the subsequent delignification rate. Furthermore, a methodology developed by Brännvall and Rönnols [8] was employed to partition the black liquor into two distinct fractions: the bulk liquor (BL) surrounding the chips, and the liquor entrained within the lumen network (centrifuged liquor, CL). Varying the impregnation liquor composition resulted in a small but consistent divergence between the impregnation scenarios, which persisted throughout the cooking process, as presented in *Figure 1* of Paper III. As expected, impregnation with liquor containing OH^- and HS^- accelerated delignification compared to impregnation with water alone.

Despite the initial scope, the liquor fractionation yielded unexpected findings, prompting a shift in focus for the remainder of the study. The concentrations

of dissolved Klason lignin and xylan are presented in Figure 5.11, illustrating two distinct kinetic behaviours when comparing the two liquor fractions. For both components, the overall trends were comparable, although the specific dissolution rates and peak times varied consistent with the behaviours observed in the pulp (cf. *Figure 1* of Paper III). For example, the lignin concentration in the bulk liquor steadily increased during the first 60 minutes, after which the rate was drastically diminished, causing the concentration profile to level off. Conversely, the centrifuged fraction exhibited a steeper initial increase, reaching a maximum concentration concurrent with the levelling off of the bulk liquor, followed by a decrease for the remainder of the cook.

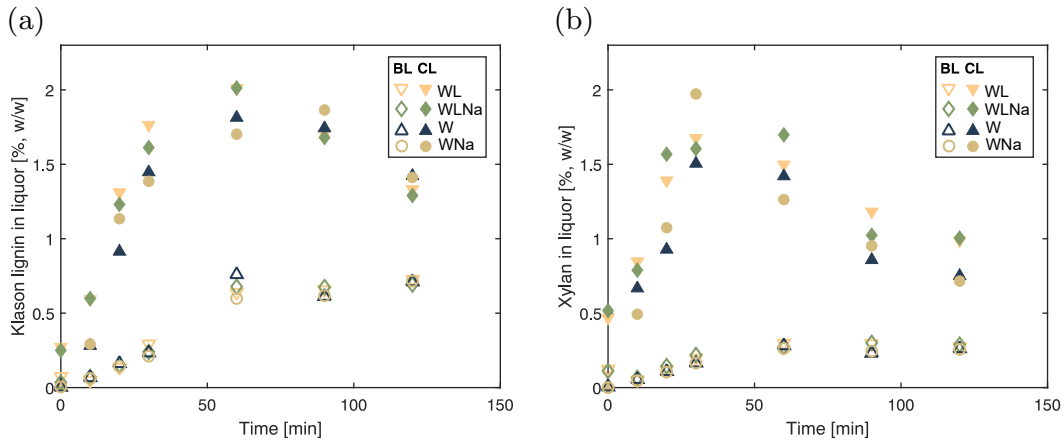

Figure 5.11: Concentration of dissolved (a) Klason lignin and (b) xylan in the bulk liquor (BL, open symbols) and centrifuged liquor (CL, closed symbols) during pulping, following the impregnation with: White liquor (WL), White liquor with added NaCL (WLNa), Water (W), and Water with added NaCL (WNa)

The disparity in concentration between the bulk and centrifuged liquors indicates substantial transport resistance within the chip; if mass transfer between the two phases were unhindered, their concentrations would instead have been expected to rapidly equilibrate to similar levels.

Moreover, the observation of maxima in the CL concentration profiles suggests that the balance between the rate of lignin release into the CL and the rate of transport from the CL to the BL varies throughout the process. During the initial phase, lignin solubilisation is rapid, causing the CL concentration to rise sharply and exceed that of the BL. However, after approximately 60 minutes, the rate of release from the wood matrix diminishes. Consequently, the CL concentration decreases as dissolved fragments continue to migrate into the bulk liquor.

Consistent with this mechanism, the MWD of lignin precipitated from the CL and BL exhibited similar disparities over time (Figure 5.12).

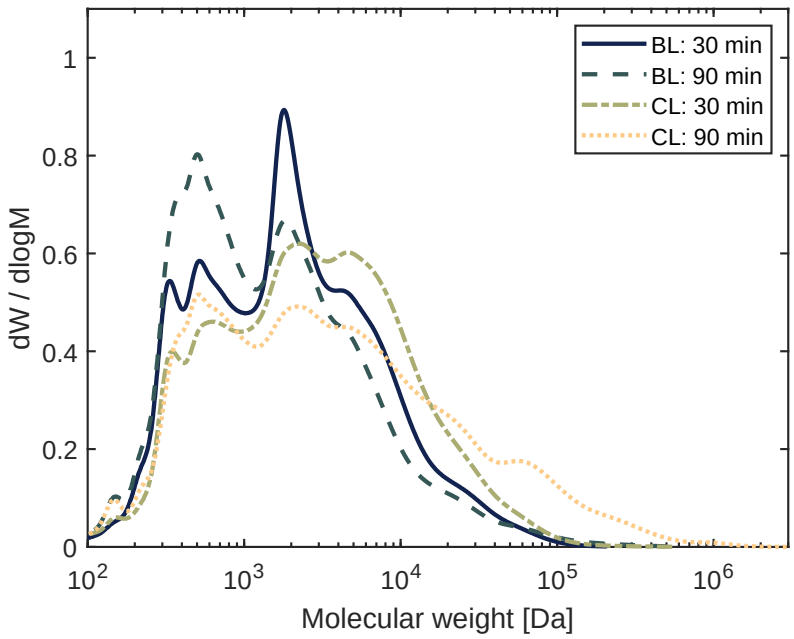

Figure 5.12: Molecular weight distribution of material precipitated from the bulk (BL) and centrifuged (CL) liquor fractions after 30 and 90 minutes of cooking of birch wood meal, as detected by UV. Cooking conditions: 160 °C, 0.60 OH^- and 0.15 HS^- ·

In the centrifuged fraction, the MWD shifted towards higher molecular weight fractions over time, paralleling the behaviour observed in Figure 5.5. In contrast, the bulk fraction exhibited a gradual decrease in molecular weight over time. This trend is likely attributable to the continued degradation of larger fragments within the bulk liquor, a phenomenon that was effectively minimised in the wood meal experiments due to the immediate sampling and cooling of the flow-through liquor. Similar reductions in molecular weight have been reported previously [8, 10]. Furthermore, irrespective of the sampling time, the CL consistently contained larger lignin fragments, which further corroborates the existence of transport limitations between the two phases.

These trends in wood chip pulping largely align with the findings from the wood meal studies, hinting towards the same progression of delignification mechanisms: initially, rapid reactions occurred, solubilising lignin fragments of various sizes—the smaller of which were quickly removed. After approximately 60 minutes, the reaction rate diminished markedly, and the subsequent lignin removal was primarily governed by the diffusion of the remaining larger fragments. Notably, the remaining lignin after 60 minutes was similar in both wood-meal and chip experiments—about 4% (w/w on wood). However, differences in factors such as the temperature profile and local alkali availability affects the specific kinetics of each situation, so the two should be compared with caution.

5.3 Cell wall delignification model

5.3.1 Model development

A delignification model was developed with the objective of capturing the continuously evolving MWD profile of the dissolved lignin. Predicated on the hypothesis that the observed MWD behaviour arises from the diffusion of a heterogeneous mixture of lignin fractions with varying mobilities, the model partitioned the lignin into two distinct categories: the unreacted lignin, L_S, which remains bound to the lignocellulosic matrix; and the dissolved lignin, $L_{D,i}$, which represents fragments liberated from the matrix that are non-reactive and free to diffuse from the cell wall.

Many prior delignification models, such as the Gustafson or Purdue model families [131, 133], employ complex rate expressions—often involving distinct fast- and slow-reacting components—to capture the kinetics of kraft delignification. However, these models typically neglect the transport of dissolved wood components, a factor explicitly incorporated into the model developed in this work. Consequently, it was deemed sufficient to describe the reaction of unreacted lignin—converting it into the dissolved fractions $L_{D,i}$—via a simple, pseudo-first-order rate expression, as defined in Equation 5.1,

$$\frac{\delta L_S}{\delta t} = -r_L = -L_S \left[\frac{OH}{OH_0}\right] A_r e^{-E_r/RT} \tag{5.1}$$

where r_L is the reaction rate, A_r is the pre-exponential factor, E_r the activation energy, and R the thermodynamic gas constant. The model was developed prior to the insights reported in Paper II, which nevertheless demonstrated that the specific role of HS^- in delignification kinetics is complex and warrants further investigation. Consequently, the dependence of the rate expression in Equation 5.1 on HS^- was not explicitly represented. Instead, the experimental conditions used for model validation were selected such that only minor variations in the HS^- concentration were expected, allowing its influence on the reaction rate to be treated as effectively constant.

The Stokes-Einstein theory predicts that diffusivity is inversely proportional to the hydrodynamic radius, thereby implying an inverse scaling relationship with molecular weight (see Equation 5.2):

$$D = \frac{k_B T}{6\pi\mu r_H}, \qquad \text{where} \quad r_H \propto {M_W}^{\alpha} \tag{5.2}$$

where, k_B is the Boltzmann constant, μ the viscosity of the solvent, and r_H the hydrodynamic radius of the molecule which relates to the molecular weight by the factor α. This factor depends on the configuration of the dissolved lignin in the solvent [72] and was set to 0.5 in this work. Given the dependence on molecular weight in Equation 5.2, the dissolved fraction was discretised into seven sub-fractions, defined according to the MWD data presented in Figure 5.5(b). Each fraction was assigned a diffusivity scaled to its

corresponding molecular size, $D_{L_D i}$. Furthermore, a temperature dependence was incorporated based on the expression developed by McKibbins [63], yielding the following relationship:

$$D_{L_{Di}} = D_0 \sqrt{\left(\frac{T}{T_0}\right)} e^{-E_D/RT} \left[\frac{\mathrm{OH}}{\mathrm{OH}_0}\right]^m w_i^{-0.5} \tag{5.3}$$

where D_0 is a factor analogous to the frequency factor, E_D the activation energy of diffusion, and w_i the relative weight of each fraction ranging from 1–2930.

In addition to lignin, the evolution of the OH^- concentration was simulated. The diffusivity was set to 10^{-11} m^2/s (independent of temperature), based on estimates of water diffusion in cellulose micropores [79]. The majority of OH^- consumption arises from carbohydrate reactions, which were not explicitly included in the model formulation. To address this, a linear correlation between alkali consumption and carbohydrate content was combined with a corresponding linear correlation between carbohydrate degradation and lignin removal—a methodology that has previously yielded satisfactory results [13, 131, 133, 134].

The initial conditions assumed a uniform distribution of OH^- equivalent to the bulk concentration, and that all lignin initially belonged to the L_S fraction. Furthermore, the boundary conditions were formulated based on simplified transport across a linear gradient extending from the cell wall surface to the boundary of an idealised *lumen* exposed to the bulk liquor.

5.3.2 Parameter fitting and Model validation

Experimental validation of the physicochemical properties governing kraft delignification is inherently challenging. This difficulty arises partly from the complexity of decoupling simultaneous mechanisms to isolate individual contributions, and partly from the heterogeneous structure of wood, which implies that the local chemical environment—and thus the material properties—varies significantly across different length scales. While numerous studies have reported rate constants for kraft delignification [131, 133, 137], these values often fail to decouple transport phenomena from reaction kinetics. Consequently, they represent the *apparent* rates rather than the *intrinsic* reaction rates. Similarly, the estimation of lignin diffusivities is highly sensitive to the experimental configuration, with reported values spanning several orders of magnitude [74, 77, 79]. Therefore, five parameters governing reaction kinetics (A_r, E_r) and diffusivity (D_0, E_D, m) were determined by fitting the model to experimental data. The experimental conditions covered a range of 0–180 minutes, 140–160°C, and 0.35–0.7 M OH^-, with HS^- maintained constant at 0.15 M.

Figure 5.13(a) illustrates the close agreement between the experimental data and the model response, yielding an overall R^2 value of 0.997[1]. Naturally, as the experimental data in Figure 5.13(a) were utilised for parameter estimation, this figure represents a fit rather than a demonstration of predictive behaviour. To assess the model's predictive capabilities more rigorously, independent experimental data were acquired that were not included in the fitting process. Furthermore, these data were obtained under transient process conditions to challenge the model's robustness.

As demonstrated in Figure 5.13(b), the model exhibited excellent predictive performance, achieving an average R^2 value of 0.986 across all independent validation sets.

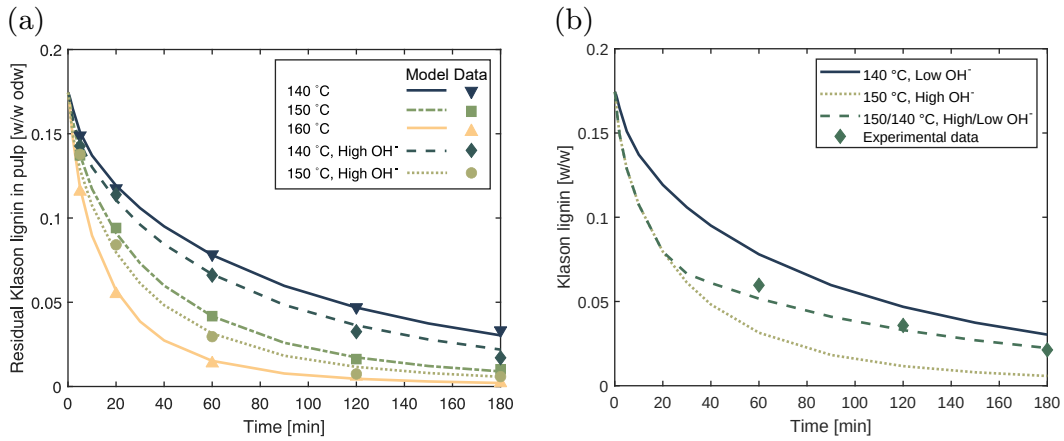

Figure 5.13: (a) Fitted and (b) predicted (lines) versus experimental (points) decrease in the total Klason lignin content of the pulp after delignification at different process conditions. For the transient conditions (dark green dashed line in (b)), the switch between the indicated conditions occurred after 20 minutes. Lignin content is normalized to the initial content in the wood.

The predicted evolution of the MWD is illustrated in Figure 5.14(a), where it is compared to the experimental data initially presented in Figure 5.5(b). The simulated MWD showed strong consistency with the experimental results for the smaller fragments ($< 5 \times 10^4$ Da), which correspond to more than 95% of the total dissolved lignin. In contrast, the model did not accurately predict the dominance of the largest fractions ($> 10^5$ Da) observed after 120 minutes. This deviation is partly explained by the model formulation: the average MWD utilised as the basis for the model was derived from dissolved lignin. Consequently, this distribution is inherently biased towards smaller fractions, as it excludes the high-molecular-weight populations that remain bound within the cell wall until the later stages of delignification. Furthermore, the simulations rely on the scaling parameter relating molecular weight to hydrodynamic radius (α in Equation 5.2). Experimental work have reported values corresponding

[1]The simulated results are updated based on the normalization procedure employed in Paper V. For the original figures, refer to appended Paper IV.

to an α as high as 1.2, in contrast to the 0.5 used in the present work [79]. A higher α would imply a stronger dependence of diffusivity on molecular weight, which would theoretically account for the increased abundance of larger fractions in the MWD at later reaction times.

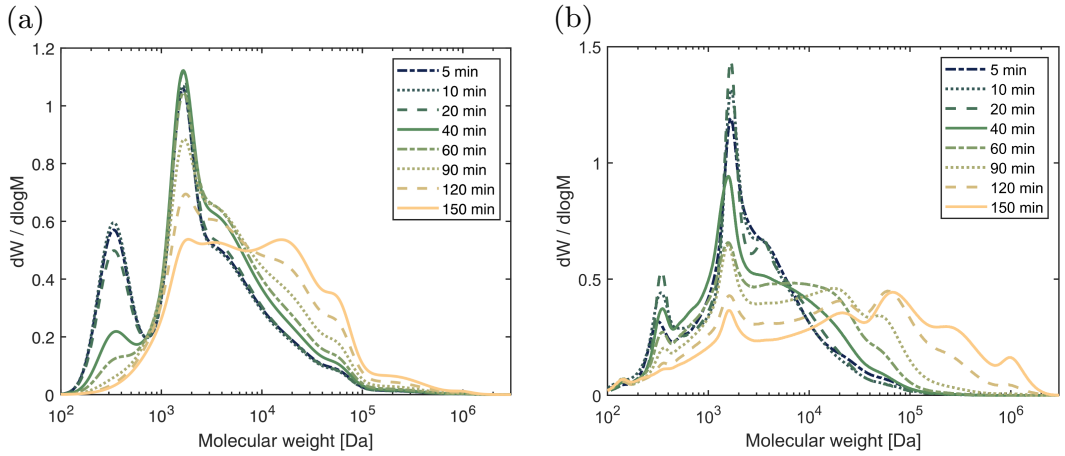

Figure 5.14: Molecular weight distribution of precipitated lignin as (a) simulated by the model and (b) experimentally measured during cooking at 150°C. CC-BY [162]

5.3.3 Predicted Delignification behaviour

The estimated values for the fitted parameters are presented in Table 5.2. The obtained reaction rate is considerably faster than the *apparent* reaction rates typically reported in the literature [108, 140, 163]. However, the *intrinsic* reaction rate is likely better compared with values derived from model compounds. While some studies report rates slower than those listed in Table 5.2 [90, 164], others report values in a comparable range [102].

To my knowledge, there are no reported values for lignin diffusivities specifically under kraft pulping conditions. However, estimates based on the washing of kraft pulp exist; when extrapolated to the temperatures employed in this work, these values fall within the same order of magnitude as those reported herein [76, 77]. A sensitivity analysis of all *a priori* defined parameters demonstrated the model's robustness; significant variations in the fitted parameters (Table 5.2) were observed only when perturbing process parameters explicitly involved in their calculation (refer to the *Supplementary Information* of Paper IV).

Table 5.2: Calculated values for the process parameters assigned through regression[a]

A_r [s^{-1}]	E_r [kJ/mol]	D_0 [m^2/s]	E_D [kJ/mol]	m
2.2×10^5	56.9	1.4	118.3	0.357
(2.3×10^5)	(56.9)	(1.5)	(118.5)	(0.352)

Calculated reaction rate and diffusivity at 150 °C, 0.35 M OH^- and $L_s = 1$:

$r_L = 2.1 \times 10^{-2}$ s^{-1}	$D_{L,Di} = 6.4\text{–}350 \times 10^{-17}$ m^2/s
$(r_L = 2.1 \times 10^{-2}$ $s^{-1})$	$(D_{L,Di} = 6.5\text{–}350 \times 10^{-17}$ $m^2/s)$

[a] Values are updated based on the normalization procedure applied in Paper V. Original values as reported in Paper IV included in parenthesis.

The simulated concentration surfaces of four distinct components are presented in Figure 5.15[2]. Consistent with the rapid reaction rate reported in Table 5.2, the solid lignin (L_S) was converted at an exceptionally high rate, achieving full solubilisation within 5 minutes (Figure 5.15(a)). The OH^- concentration followed a similar, albeit inverted, trajectory. Notably, further investigations revealed that increasing the selected OH^- diffusivity enhanced the conversion of L_S, which corresponds to a reaction that is—at least partially—limited by alkali supply. Nevertheless, both mechanisms proceed relatively rapidly compared to the diffusion of the dissolved lignin fractions. Even the smallest fraction (Figure 5.15(c)) was removed at a slower rate than L_S. As anticipated, diffusion rates decreased with increasing molecular weight (M_w), as illustrated in Figure 5.15(d).

Consequently, a significant quantity of the larger lignin fractions remained within the cell wall after 180 minutes according to the simulation. This transport-controlled behaviour offers a plausible explanation for the slow delignification rates typically observed during the final phase of pulping [115], a phenomenon otherwise commonly attributed to condensation reactions [165].

[2]The simulated results are updated based on the normalization procedure employed in Paper V. For the original figure, refer to appended Paper IV.

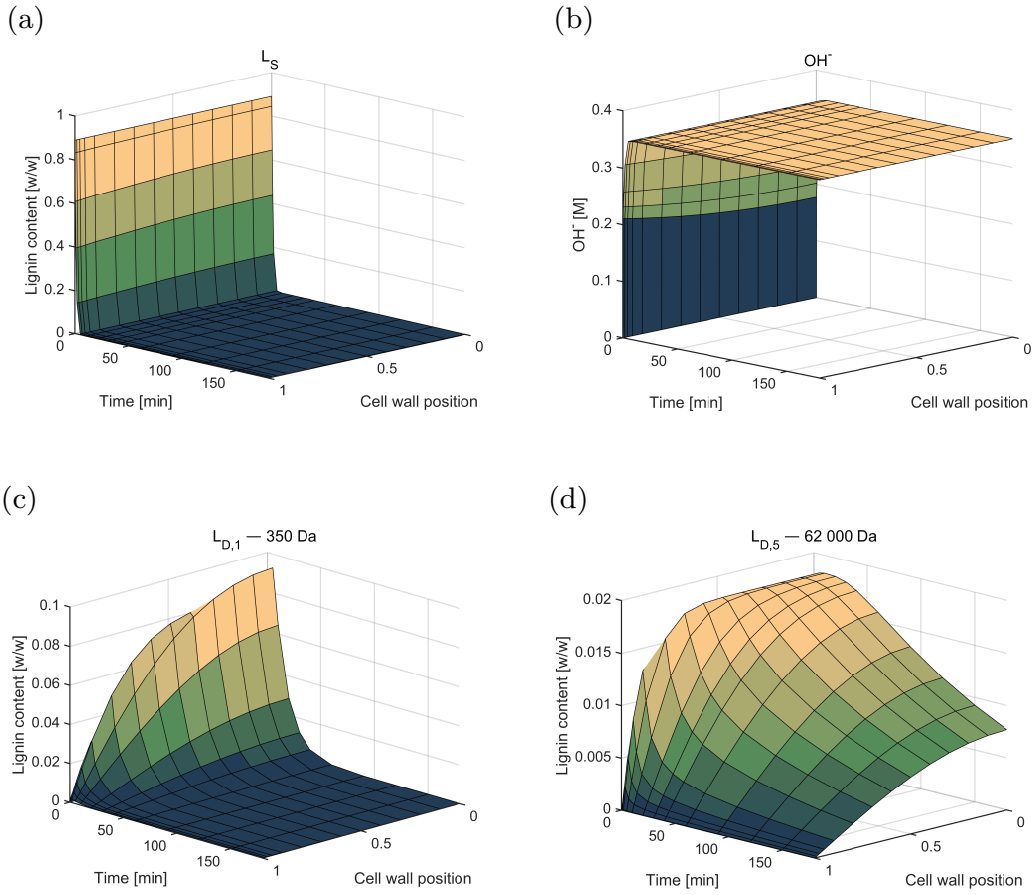

Figure 5.15: Simulated cell wall concentrations of (a) unreacted lignin, (b) OH^-, (c) dissolved lignin (350 Da fraction), and (d) dissolved lignin (62 kDa fraction) during cooking at 150°C with an OH^- concentration of 0.35 M.

5.3.4 Applicability of the model

Although the developed model predicted a reaction rate considerably higher than that traditionally reported, the absolute values should be interpreted with caution. The parameters listed in Table 5.2 are strongly influenced by both the experimental configuration and the structural assumptions embedded within the model. Instead, their principal value lies in the relative comparison of governing mechanisms (i.e., reaction versus diffusion) rather than in providing universally applicable physical constants. Establishing such generalised data would require further experimental studies specifically designed to decouple these phenomena.

Consequently, the primary conclusion drawn from the simulation results is that, contingent upon the current model structure, the best fit between experimental data and model response corresponds to a process in which the diffusion of dissolved lignins is considerably slower than the chemical reaction liberating them.

However, alternative model formulations might yield differing outcomes. For

instance, the results presented in Section 5.1.1 suggested that reactions involving HS^- persisted for at least 60 minutes, a duration considerably exceeding the 5 minutes predicted by the current model. Incorporating additional reaction pathways would enable the model to encompass both rapid reactions—such as the cleavage of phenolic β-O-4 linkages—and slower mechanisms, such as demethylation. Nevertheless, demethylation merely promotes the dissolution of large lignin fragments, which still need to be removed. The model outcome therefore remains consistent with the findings in Section 5.1.1, which highlight the governing role of the slow diffusion of these fragments during the final stages of delignification.

5.4 Wood chip delignification model

5.4.1 Model structure

The framework presented in Section 5.3 was subsequently embedded into a one-dimensional, multi-scale model describing the delignification kinetics across the thickness of birch wood chips. The core premise of this model was that, at the macroscopic chip level, the *apparent* reaction rate represents the cumulative effect of the *intrinsic* reaction kinetics and the diffusion of lignin from the cell wall, as described in Section 5.3. Consequently, the wood chip was discretised into N macroscopic segments, where the delignification rate of each segment was governed by the conditions within a single representative fibre. Given that the cell wall model accounts for spatial heterogeneity and is driven by intra-wall concentration gradients, each representative fibre was further discretised into M radial layers. A schematic illustration of the model geometry is presented in Figure 5.16.

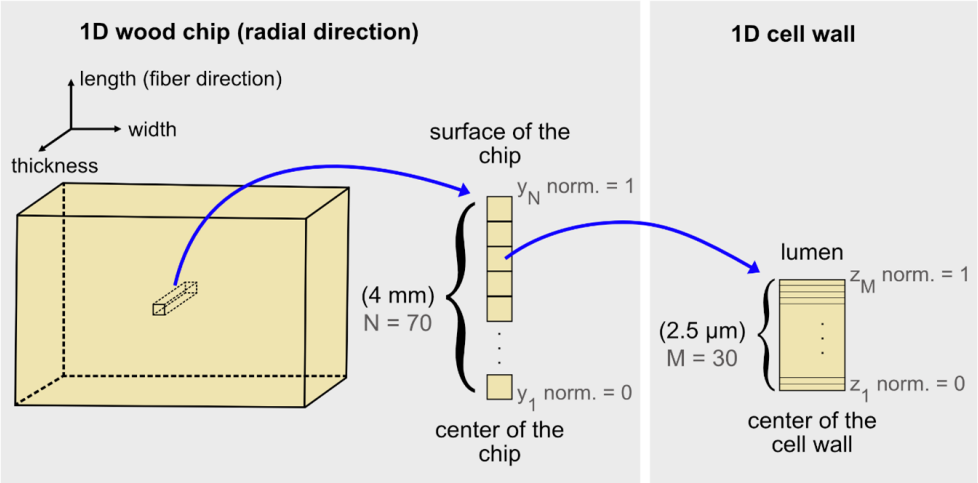

Figure 5.16: Schematic representation of the model geometry, representing (left) wood chip segments and (right) cell wall layers.

The model structure comprised two distinct hierarchical levels. At each time step, the first level—describing delignification within the M radial layers of

each wood chip node—was solved in a manner analogous to the original cell wall model. The primary modification is regarding the boundary conditions, which were updated to the local liquid phase concentrations within each of the N macroscopic chip segments, rather than the constant bulk liquor properties. The resulting total flux of lignin and OH^- across the boundary of each fibre node (representing mass transfer from the cell wall into the lumen) was subsequently utilised as the *apparent* reaction rate for the second level. This second level simultaneously governed the macroscopic transport of OH^- along the wood chip thickness. For a comprehensive description of the model architecture, refer to Paper V.

The transport of dissolved wood components was excluded from the model at the wood chip level. The reason being that the dissolved components will accumulate in the lumen with limited impact on the continued delignification within the cell wall. In addition, the experimental data to which the model would be compared was based on washed and subsequently leached wood chips. Therefore, any lignin remaining dissolved in the lumen would be largely removed, and its impact on the quantified total residual lignin content would therefore be limited.

Furthermore, the wood chip model incorporated a more rigorous description of OH^- diffusivity. This diffusivity was estimated using the Nernst-Haskell equation, wherein the limiting ionic conductance was correlated with the viscosity of water, μ_{H_2O}, thereby establishing the temperature dependence defined in Equation 5.4.

$$D_{\mathrm{OH,free}} \propto \frac{T}{\mu_{H_2O}} \tag{5.4}$$

The free diffusivity, $D_{\mathrm{OH,free}}$, was applied to the boundary conditions governing the bulk liquor and the transport within the lumen space. However, for diffusion across the lumen network (i.e., along the chip thickness), $D_{\mathrm{OH,free}}$ was modified by the *Effective Capillary Cross Sectional Area* (ECCSA). This factor, which accounts for structural tortuosity and pore availability, varies with pH according to the findings of Stone [67]. Specifically, in the radial direction, the ECCSA remains constant at approximately 0.1 for pH levels up to 12, beyond which it rises to roughly 0.4 at pH 14. Conversely, in the longitudinal direction, the ECCSA is constant ($\sim$0.5) across the entire measured pH range. For transport within the cell wall matrix, the OH^- diffusivity was alternatively corrected using the McKibbins expression [63]. This formulation introduces a square-root-exponential temperature dependence, providing a description more suitable for hindered diffusion within the solid matrix [166].

5.4.2 Model response

Initially, two scenarios were evaluated for the starting OH^- concentration. The first case assumed complete impregnation with negligible alkali consumption prior to the reaction onset (0.55 M), while the second scenario adopted

the lowest concentration empirically measured within the wood chips post-impregnation (0.06 M). In both instances, a uniform spatial distribution was assumed. Figure 5.17 presents selected simulation results from these two scenarios, benchmarked against experimental data reported by Marion de Godoy et al. [148].

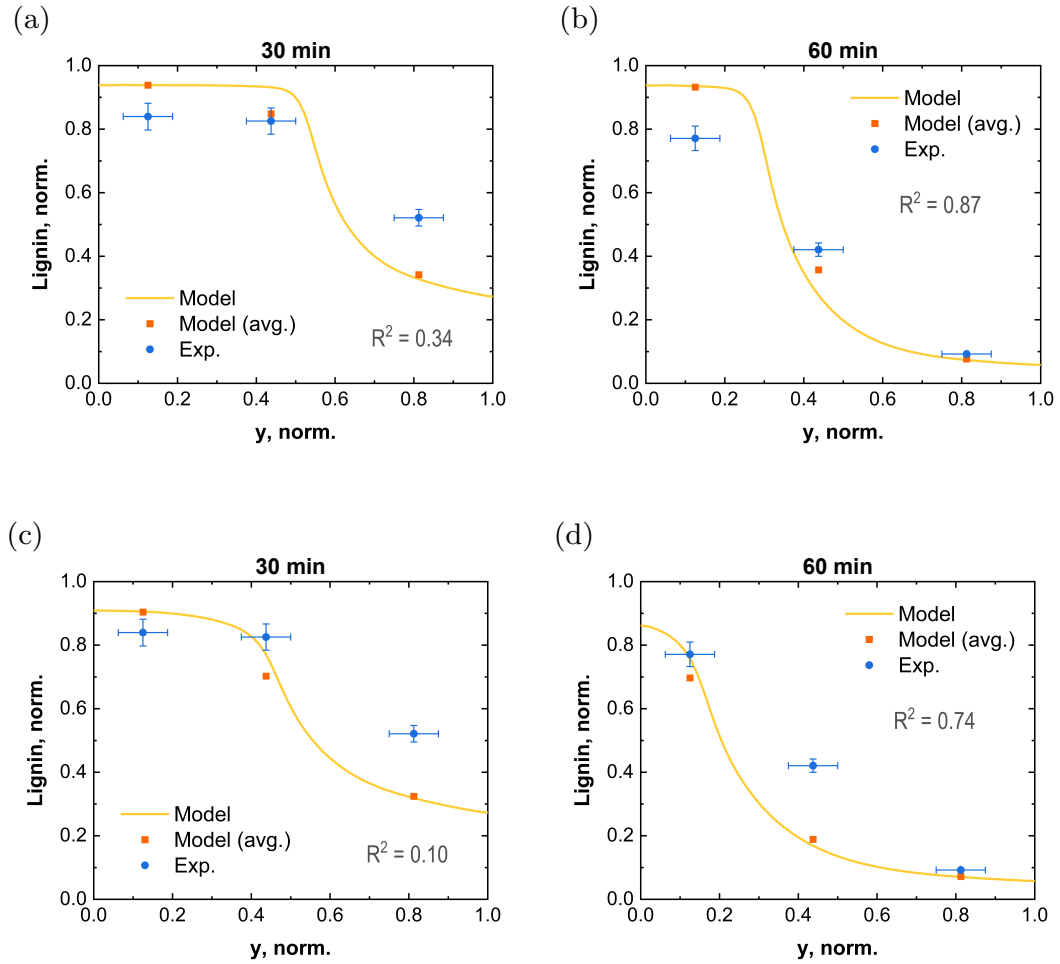

Figure 5.17: Normalized lignin content across the radial direction in the middle of the wood chip, as simulated by the model using (a & b) $OH_0 = 0.06M$ and (c & d) $OH_0 = 0.55M$. Blue asterisks represent experimental data; red squares represent simulated data (line) averaged across the same segments as the experimental data.

As illustrated in Figure 5.17, the initial concentration of OH^- had a considerable influence throughout the entire cook. Notably, the discrepancy between the two scenarios widened over time, even at the centre of the wood chip (cf. the left-most data points in Figure 5.17). Interestingly, in both cases, the OH^- was completely depleted at the chip centre after approximately 10 minutes, as inferred from the horizontal gradient observed in the upper-left corners of Figures 5.18b and 5.18d. This implies that the direct kinetic benefit of higher initial OH^-—which enables more extensive delignification prior to depletion—should theoretically distinguish the scenarios only during these first 10 minutes.

Conversely, the prolonged divergence observed in Figure 5.17 must stem from a sustained secondary mechanism. One plausible explanation is that higher pH levels increase the ECCSA, thereby enhancing alkali diffusion into the chip. This effect is visible in Figure 5.18, where the OH^- gradient penetrates deeper into the chip structure in Figure 5.18d compared to Figure 5.18b.

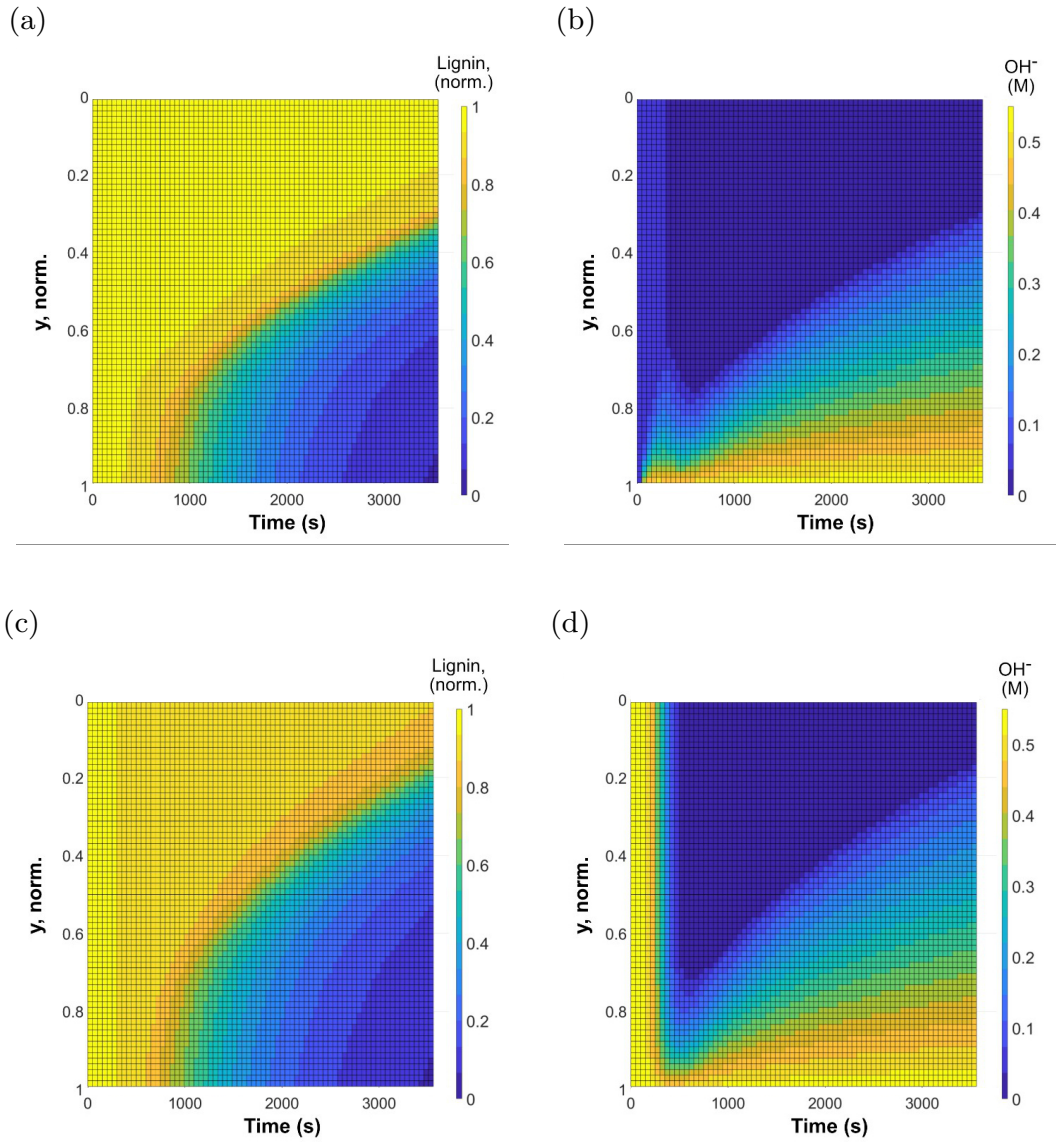

Figure 5.18: Simulated wood chip concentrations of (a & c) remaining lignin and (b & d) OH^-, as simulated by the model using (a & b) $OH_0 = 0.06M$ and (c & d) $OH_0 = 0.55M$.

Furthermore, the concentration profiles for lignin (Figures 5.18a and 5.18c) exhibited an inverse, yet complementary, pattern to those of OH^- (Figures 5.18b and 5.18d). This correlation suggests that the reaction kinetics are spatially constrained by alkali availability; otherwise, delignification would presumably proceed more uniformly across the chip cross-section. In addition, apart from the initial delignification near the surface, the lignin concentration formed a steep profile that propagated inward over time, whereas the concentration gradient of OH^- remained approximately linear.

These simulation results suggest that hydroxide diffusion was slow relative to its consumption and consequently limited the reaction rate.

Moreover, the nearly horizontal gradient observed near the surface in the simulation (close to $y = 1$ in Figures 5.18a and 5.18c) further suggests that relatively uniform delignification could be achieved by reducing the chip thickness to approximately 30% of the dimension used in this study (i.e., 2–3 mm) under similar conditions. Similarly, comparisons with experimental data along the longitudinal axis revealed an even (relatively) larger fraction of undelignified material (cf. *Figure 10* in Paper V). This observation underscores chip thickness as the critical parameter governing pulping uniformity and justifies its selection as the representative geometric dimension for the model.

5.4.3 Sensitivity analysis

Several uncertainties associated with the model assumptions and parameter values were identified, primarily related to factors governing alkali availability (see Paper V for details). Addressing these uncertainties, the agreement between model predictions and experimental data could be improved through two principal modifications.

First, to address the overestimation of delignification at the chip surface (cf. the rightmost data in Figures 5.17a and 5.17c), the ECCSA was redefined from a pH-dependent variable to a constant value within the relevant range. These changes reflect deviations between the data from Marion de Godoy *et al.* and the experimental conditions applied during the original estimation of the ECCSA, in terms of time scale and employed feedstock.

Second, the *intrinsic* reaction rate of the original cell wall model was decreased approximately fourfold (corresponding to a characteristic reaction time of about 20 minutes at 150°C). This was accompanied by a simultaneous increase in the diffusivities of the dissolved lignin fractions, thereby maintaining the *apparent* reaction rate at an essentially constant level. This latter modification aimed to correct the underestimated delignification predicted at the chip centre (cf. the leftmost data in Figures 5.17a, 5.17b, and 5.17c) by effectively reducing the local rate of OH^- consumption, thus enabling greater alkali penetration into the chip core. The combined effect of these adjustments yielded considerable

improvements to the model's agreement with experimental data, as illustrated in Figure 5.19.

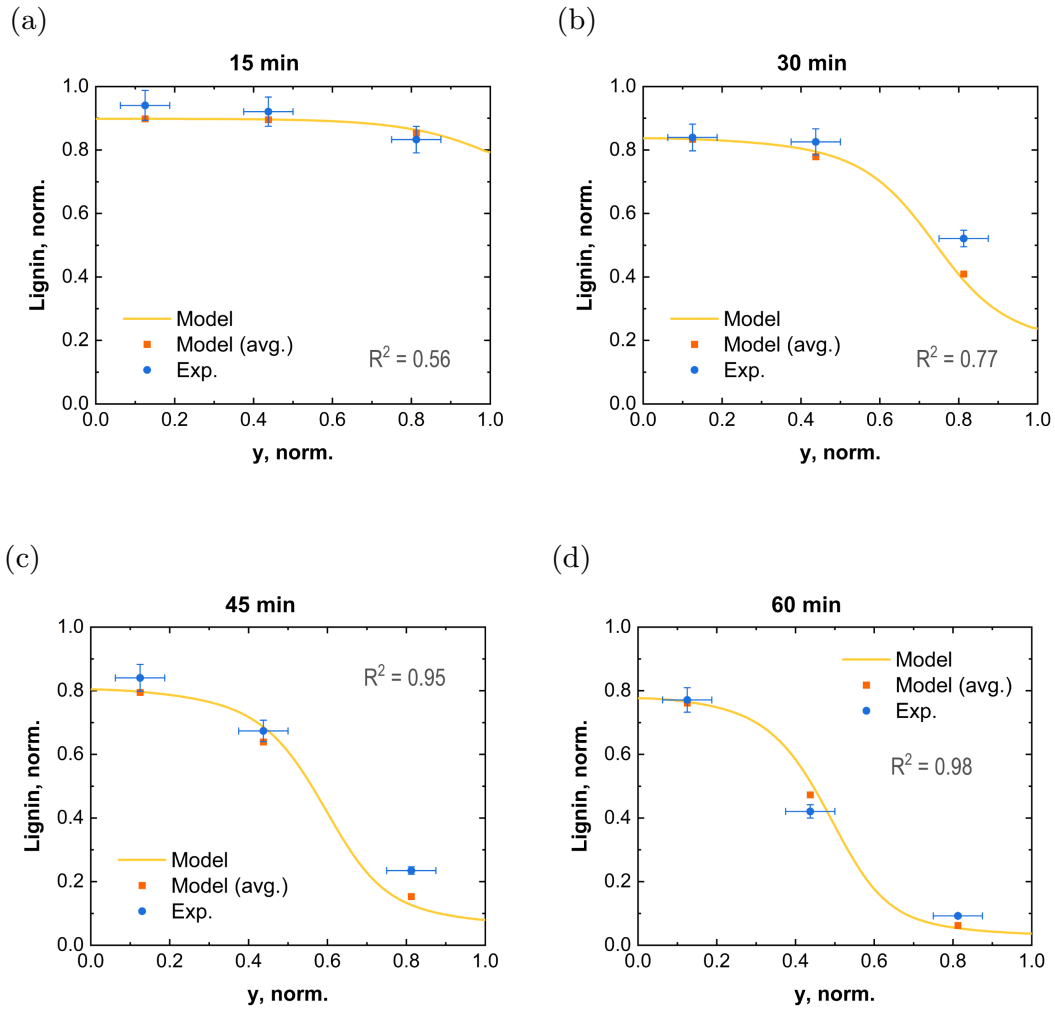

Figure 5.19: Normalized lignin content across the radial direction in the middle of the wood chip, as simulated by the model using modified parameters: $OH_0 = 0.31M$, ECCSA=0.2, and a decreased *intrinsic* reaction rate.

Importantly, the modified parameters do not represent more accurate estimates of the underlying physical properties, nor do they constitute an optimal parameter set with respect to agreement with experimental data. Rather, the results demonstrate that the developed model is capable of reproducing the experimental observations with high precision. However, this performance exhibits a strong dependence on several physical parameters—many of which rest on relatively uncertain empirical grounds—that are directly connected to alkali availability at the chip level.

These findings underscore the importance of accounting for alkali availability within wood chips throughout the entire delignification process, rather than considering it only during the initial impregnation stage.

Chapter 6

Concluding remarks

This thesis highlights the inherent complexity of kraft delignification kinetics. It shows that the process cannot be described as a simple, homogeneous reaction; rather, it arises from an intricate interplay of mechanisms involving multiple rate-affecting reactions and mass transport of alkali and lignin, each having distinct influences across different length scales.

Wood-meal experiments—representing the pulping of exposed cell walls—demonstrated that the delignification rate depends on several reaction pathways. While the initial liberation of lignin from the lignocellulosic matrix is likely dominated by cleavage of β-O-4 linkages, the results also indicate contributions from other reactions, such as demethylation of methoxy groups. These pathways generate a highly heterogeneous dissolved lignin fraction, which was found to span nearly four orders of magnitude in molecular weight. Moreover, the evolution of this molecular-weight distribution suggests that, although small and mobile fragments are rapidly extracted from the cell wall, larger species diffuse far more slowly and ultimately limit the overall delignification rate during the later stages.

In wood chip pulping, the cell wall accessibility is no longer uniform, and large discrepancies were found to exist between the liquor environment within the chips and that of the surrounding bulk, indicating that the diffusion is limiting the overall kinetics. Consequently, the availability of alkali is likely a critical factor at this level and, depending on the chip thickness, may generate heterogeneous concentration profiles and lead to non-uniform pulping.

Finally, a delignification model was developed that introduced a novel approach to representing lignin heterogeneity by linking diffusion kinetics to molecular weight. The model was then extended to enable simultaneous simulation of heterogeneous delignification at both the cell-wall and chip scales. Although the models remain constrained by uncertainties in key physicochemical parameters—many of which are inherently difficult to determine experimentally, such as the strongly condition-dependent diffusivity of lignin and the stoichiometric

consumption of alkali—they nonetheless advance process understanding by clarifying the influence of these parameters on overall delignification behaviour. Importantly, the models demonstrates good agreement with experimental data and the capability to predict transient delignification behaviour, indicating the potential for improved process simulation when diffusional phenomena are explicitly incorporated.

6.1 Future Work

Despite these advances, several aspects of the governing mechanisms of kraft delignification remain unresolved and require further investigation. One area that warrants particular attention is the role of HS^-. While its importance in kraft pulping is well established, the results of this thesis suggest that sulphide may influence delignification kinetics through pathways that have not yet been fully explored. In particular, further validation of lignin-demethylation kinetics and their implications for lignin solubility, could provide valuable insight into the coupled reaction–transport processes involved.

The present work has focused primarily on the characterisation of dissolved lignin. To obtain a more complete description of delignification kinetics, complementary structural characterisation of the residual lignin remaining in the pulp is required. Although initial efforts in this direction have been reported [167–169], further studies are needed to resolve the effects of species variation and pulping conditions. In particular, finer temporal sampling during cooking would enable the full kinetic progression of delignification to be captured. Such efforts also motivate the development of refined isolation protocols for residual lignin that minimise structural alteration while remaining applicable to highly delignified pulps.

In addition, the influence of transport phenomena on delignification kinetics remains incompletely described across multiple length scales. Recent advances using *in situ* X-ray tomography have demonstrated the potential to interrogate micro- and nanoscale structural and chemical changes during pulping, including variations in porosity and cell wall thickness, although this research area is still in a stage of development [119]. Extending such approaches to the chip scale would be equally valuable, particularly to elucidate how anisotropic transport of dissolved wood components evolves as delignification progresses.

Looking ahead, future modelling efforts should aim to adopt a more holistic description of kraft delignification. Such models would need to account for the presence of multiple dissolved species with distinct transport and solubility characteristics, the continuous evolution of the multiscale lignocellulosic network, and the interplay between parallel reaction pathways and alkali consumption. While the development of comprehensive models of this nature is inherently challenging, incremental progress is expected to yield an improved understanding of the complex process of kraft delignification.

Acknowledgements

The financial support of the Resource-smart Processes network, financed by Vinnova via Bioinnovation and industrial partners (Billerud, Holmen, SCA, Stora Enso, Södra Skogsägarna and Valmet), is gratefully acknowledged. Attendance to several conferences has also been made possible through stipends from the following: Nils Pihlblads stipendiefond, Bo Rydins stiftelse, Gunnar Sundblads forskningsfond, Chalmerska Forskningsfonden, and Marcus Wallenberg foundation.

I would also like to sincerely thank the following people who enabled the completion of thesis—either directly, or simply by making the journey more enjoyable:

- **Merima Hasani**, my main supervisor. Beginning my Masters' studies, I was completely certain that the paper industry was old, uninteresting and stinky. Safe to say, you had me completely converted by the end of your biorefinery class. You have always been supporting, positive, and thoughtful, and while PhD studies can be daunting, it have felt less so with you as my supervisor.

- **Hans Theliander**, my co-supervisor. Official titles aside, in practice I have had two main supervisors. Your dedication, encouragement and vast knowledge have truly been irreplaceable, and you always seemed to find something interesting in my results, even when I doubted.

- **Carolina Marion de Godoy**, co-author, lab buddy, and travel companion. We started the PhD journey together. Now, 2 joint papers, 6 RSP courses, and 10+ trips to conferences and meetings later, were almost there! You have been a steady anchor throughout this journey, always giving your time and thought to the people around you.

- **Fredrik Wernersson Brodin** and **Espen Ribe**, for supplying the wood chips and logs this entire work has been based on.

- **Michael Andersson** and **Patrik Skansen**, for enduring the last-minute orders of lab supplies and for the skilful know-it-all work, not a single lab would be running for long without your aid.

- **Johanna Spång** and **Malin Larsson**, for all the administrative help, and for doing all the "little things", from fikas and quizzes, to coffee orders and IKEA runs.

✧ **Ulrika Brath** and others at the Swedish NMR Centre, for your help in running the experiments and for addressing all the confused questions that followed.

✧ To everyone else at **SIKT**, **KART**, and **TK**, past and present, for sharing discussions, food, and laughter, making working here much more fun.

✧ To people within the **RSP network**, for all fruitful discussions, interesting presentations, and all the fun in between.

And finally, I would like to express my deepest appreciation for the love and company of my family and friends, whose support has often taken the form of helping me *not* think about work when I am with you. This holds especially true for my wife, Olivia. You were even happier than I was when I first got this position, and perhaps even more relieved now that it is coming to a close. You make everything in life feel easier—including the writing of this thesis.

Bibliography

1. IPCC. in *Climate Change 2021: The Physical Science Basis. Contribution of Working Group I to the Sixth Assessment Report of the Intergovernmental Panel on Climate Change* (eds Masson-Delmotte, V *et al.*) 3–32 (Cambridge, United Kingdom and New York, NY, USA, 2021). doi:10.1017/9781009157896.001.
2. Okolie, J. A., Nanda, S., Dalai, A. K. & Kozinski, J. A. Chemistry and Specialty Industrial Applications of Lignocellulosic Biomass. *Waste and Biomass Valorization* **12,** 2145–2169. doi:10.1007/s12649-020-01123-0 (2021).
3. Biermann, C. J. *Handbook of Pulping and Papermaking* doi:10.1016/b978-0-12-097362-0.x5000-6 (Elsevier, 1996).
4. Sjostrom, E. *Wood Chemistry: Fundamentals and Applications* 1–293. doi:10.1016/C2009-0-03289-9 (Elsevier, San Diego, 1993).
5. Rahman, M., Avelin, A. & Kyprianidis, K. A review on the modeling, control and diagnostics of continuous pulp digesters. *Processes* **8,** 1–26. doi:10.3390/pr8101231 (2020).
6. Hatton, J. V. & Keays, J. L. Effect of chip geometry and moisture on yield and quality of kraft pulps from western hemlock and black spruce. *Can Pulp and Pap Assoc, Tech Sect, Proc* (1974).
7. Colombo, P, Corbetta, D, Pirotta, A & Ruffini, G. The influence of thickness of chips on pulp properties in kraft cooking. *Svensk Papperstidning* **67,** 505–511 (1964).
8. Brännvall, E. & Rönnols, J. Analysis of entrapped and free liquor to gain new insights into kraft pulping. *Cellulose* **28,** 2403–2418. doi:10.1007/s10570-020-03651-3 (2021).
9. Simão, J. P., Carvalho, M. G. V. & Baptista, C. M. Heterogeneous studies in pulping of wood: Modelling mass transfer of dissolved lignin. *Chemical Engineering Journal* **170,** 264–269. doi:10.1016/j.cej.2011.03.046 (2011).
10. Pakkanen, H. & Alén, R. Molecular mass distribution of lignin from the alkaline pulping of hardwood, softwood, and wheat straw. *Journal of Wood Chemistry and Technology* **32,** 279–293. doi:10.1080/02773813.2012.659321 (2012).
11. Mortha, G, Sarkanen, K & Gustafson, R. Alkaline pulping kinetics of short-rotation, intensively cultured hybrid poplar. English. *Tappi journal* **75,** 99–104 (1992).
12. Mattsson, C., Hasani, M., Dang, B., Mayzel, M. & Theliander, H. About structural changes of lignin during kraft cooking and the kinetics of delignification. *Holzforschung* **71,** 545–553. doi:10.1515/hf-2016-0190 (2017).

13. Gilbert, W, Allison, B, Radiotis, T & Dort, A. A simplified kinetic model for modern cooking of aspen chips. *Nordic Pulp and Paper Research Journal* **36,** 399–413. doi:10.1515/npprj-2020-0100 (2021).

14. Bijok, N., Fiskari, J., Gustafson, R. R. & Alopaeus, V. Modelling the kraft pulping process on a fibre scale by considering the intrinsic heterogeneous nature of the lignocellulosic feedstock. *Chemical Engineering Journal* **438,** 135548. doi:10.1016/j.cej.2022.135548 (2022).

15. Grénman, H. *et al.* Modeling the influence of wood anisotropy and internal diffusion on delignification kinetics. *Industrial and Engineering Chemistry Research* **49,** 9703–9711. doi:10.1021/ie101215a (2010).

16. Daniel, G. in *Volume 1 Wood Chemistry and Wood Biotechnology* (eds Ek, M., Gellerstedt, G. & Henriksson, G.) 45–70 (De Gruyter, Berlin, New York, 2009). doi:10.1515/9783110213409.45.

17. Fengel, D. & Wegener, G. *Wood* (eds Fengel, D. & Wegener, G.) doi:10.1515/9783110839654 (De Gruyter, Berlin, New York, 1983).

18. Rydholm, S. A. Pulping processes. *Pulping processes,* 1269 (1965).

19. Zhang, X., Li, L. & Xu, F. Chemical Characteristics of Wood Cell Wall with an Emphasis on Ultrastructure: A Mini-Review. *Forests* **13.** doi:10.3390/f13030439 (2022).

20. Jansson, M. B. & Nilvebrant, N.-O. in *Volume 1 Wood Chemistry and Wood Biotechnology* (eds Ek, M., Gellerstedt, G. & Henriksson, G.) 147–172 (De Gruyter, Berlin, New York, 2009). doi:10.1515/9783110213409.147.

21. Henriksson, G. & Lennholm, H. in *Volume 1 Wood Chemistry and Wood Biotechnology* (eds Ek, M., Gellerstedt, G. & Henriksson, G.) 71–100 (De Gruyter, Berlin, New York, 2009). doi:10.1515/9783110213409.71.

22. Klemm, D. *et al.* Nanocelluloses: A new family of nature-based materials. *Angewandte Chemie - International Edition* **50,** 5438–5466. doi:10.1002/anie.201001273 (2011).

23. Teleman, A. in *Volume 1 Wood Chemistry and Wood Biotechnology* (eds Ek, M., Gellerstedt, G. & Henriksson, G.) 101–120 (De Gruyter, Berlin, New York, 2009). doi:10.1515/9783110213409.101.

24. Henriksson, G. in *Volume 1 Wood Chemistry and Wood Biotechnology* (eds Ek, M., Gellerstedt, G. & Henriksson, G.) 121–146 (De Gruyter, Berlin, New York, 2009). doi:10.1515/9783110213409.121.

25. Balakshin, M. *et al.* Spruce milled wood lignin: linear, branched or cross-linked? *Green Chemistry* **22,** 3985–4001. doi:10.1039/D0GC00926A (2020).

26. Hu, Z., Yeh, T. F., Chang, H. M., Matsumoto, Y. & Kadla, J. F. Elucidation of the structure of cellulolytic enzyme lignin. *Holzforschung* **60,** 389–397. doi:10.1515/hf.2006.061 (2006).

27. Bourmaud, C. L. *et al.* Quantification of Native Lignin Structural Features with Gel-Phase 2D-HSQC0 Reveals Lignin Structural Changes During Extraction. *Angewandte Chemie - International Edition* **63.** doi:10.1002/anie.202404442 (2024).

28. Björkman, A. Isolation of Lignin from Finely Divided Wood with Neutral Solvents. *Nature 1954 174:4440* **174,** 1057–1058. doi:10.1038/1741057a0 (1954).

29. Chang, H.-m., Cowling, E. B. & Brown, W. Comparative Studies on Cellulolytic Enzyme Lignin and Milled Wood Lignin of Sweetgum and Spruce. *Holzforschung. Holzforschung* **29,** 153–159. doi:10.1515/hfsg.1975.29.5.153 (1975).

30. Argyropoulos, D. S., Sun, Y & Paluš, E. Isolation of Residual Kraft Lignin in High Yield and Purity. **28** (2002).

31. Wang, Z. & Deuss, P. J. The isolation of lignin with native-like structure. *Biotechnology Advances* **68,** 108230. doi:10.1016/j.biotechadv.2023.108230 (2023).

32. Crestini, C., Lange, H., Sette, M. & Argyropoulos, D. S. On the structure of softwood kraft lignin. *Green Chemistry* **19,** 4104–4121. doi:10.1039/c7gc01812f (2017).

33. Balakshin, M. Y. & Capanema, E. A. Comprehensive structural analysis of biorefinery lignins with a quantitative 13C NMR approach. *RSC Advances* **5,** 87187–87199. doi:10.1039/c5ra16649g (2015).

34. Zinovyev, G. *et al.* Getting Closer to Absolute Molar Masses of Technical Lignins. *ChemSusChem* **11,** 3259–3268. doi:10.1002/cssc.201801177 (2018).

35. Lancefield, C. S., Wienk, H. J., Boelens, R., Weckhuysen, B. M. & Bruijnincx, P. C. Identification of a diagnostic structural motif reveals a new reaction intermediate and condensation pathway in kraft lignin formation. *Chemical Science* **9,** 6348–6360. doi:10.1039/c8sc02000k (2018).

36. Favis, B. D., Yean, W. O. & Goring, D. A. Molecular Weight of Lignin Fractions Leached From Unbleached Kraft Pulp Fibers. *Journal of Wood Chemistry and Technology* **4,** 313–320. doi:10.1080/02773818408070651 (1984).

37. Dong, D. & Fricke, A. L. Effects of multiple pulping variables on the molecular weight and molecular weight distribution of kraft lignin. *Journal of Wood Chemistry and Technology* **15,** 369–393. doi:10.1080/02773819508009516 (1995).

38. Obiaga, T. I. & Wayman, M. Molecular weight distribution of lignin during alkaline pulping. *Sv. Papperstidn.* **76,** 699–703 (1973).

39. Demirbas, A. Energy Sources, Part A: Recovery, Utilization, and Environmental Effects Conversion of black alder (Alnus glutinosa L.) in supercritical solvents. *Energy Sources, Part A: Recovery, Utilization, and Environmental Effects,* 1393–1399. doi:10.1080/15567036.2014.949918 (2016).

40. Španić, N. Chemical and Thermal Properties of Cellulose Acetate Prepared from White Willow (Salix alba) and Black Alder (Alnus glutinosa) as a Potential Polymeric Base of Biocomposite Materials. *Chemical and Biochemical Engineering Quarterly* **29,** 357–365. doi:10.15255/cabeq.2015.2176 (2015).

41. Önnerud, H. & Gellerstedt, G. Inhomogeneities in the chemical structure of hardwood lignins. *Holzforschung* **57,** 255–265. doi:10.1515/hf.2003.039 (2003).

42. Pinto, P. C., Evtuguin, D. V. & Pascoal Neto, C. Structure of hardwood glucuronoxylans: Modifications and impact on pulp retention during wood kraft pulping. *Carbohydrate Polymers* **60,** 489–497. doi:10.1016/j.carbpol.2005.03.001 (2005).

43. Santos, R. B., Capanema, E. A., Balakshin, M. Y., Chang, H. M. & Jameel, H. Effect of hardwoods characteristics on kraft pulping process: Emphasis on lignin structure. *BioResources* **6,** 3623–3637. doi:10.15376/biores.6.4.3623-3637 (2011).

44. Vedernikov, D. N., Leontyev, L. L., Morskoy-Lemeshko, P. D. & Eltsova, L. S. Chemical Composition and Mechanical Properties of Various Parts of Birch Wood. *Khimiya Rastitel'nogo Syr'ya* **4,** 127–132. doi:10.14258/jcprm.20220411045 (2022).

45. González-Peña, M. M., Curling, S. F. & Hale, M. D. On the effect of heat on the chemical composition and dimensions of thermally-modified wood. *Polymer Degradation and Stability* **94,** 2184–2193. doi:10.1016/j.polymdegradstab.2009.09.003 (2009).

46. Gabrielii, I., Gatenholm, P., Glasser, W. G., Jain, R. K. & Kenne, L. Separation, characterization and hydrogel-formation of hemicellulose from aspen wood. *Carbohydrate Polymers* **43,** 367–374. doi:10.1016/S0144-8617(00)00181-8 (2000).

47. Josefsson, T., Lennholm, H. & Gellerstedt, G. Steam explosion of aspen wood. Characterisation of reaction products. *Holzforschung* **56,** 289–297. doi:10.1515/hf.2002.047 (2002).

48. Kron, L. *Hardwood delignification* Lic thesis (Chalmers University of Technology, 2024).

49. Germgård, U. in *Volume 2 Pulping Chemistry and Technology* (eds Ek, M., Gellerstedt, G. & Henriksson, G.) 239–276 (De Gruyter, Berlin, New York, 2009). doi:10.1515/9783110213423.239.

50. FAO. *Pulp and paper capacities, survey 2021–2026 / Capacités de la pâte et du papier, enquête 2021-2026 / Capacidades de pulpa y papel, estudio 2021-2026* tech. rep. (FAO, Rome, 2022). doi:10.4060/cc1985t.

51. Brännvall, E. & Reimann, A. The balance between alkali diffusion and alkali consuming reactions during impregnation of softwood. Impregnation for kraft pulping revisited. *Holzforschung* **72,** 169–178. doi:10.1515/hf-2017-0078 (2018).

52. Bogren, J., Brelid, H. & Theliander, H. Reaction kinetics of softwood kraft delignification - General considerations and experimental data. *Nordic Pulp and Paper Research Journal* **22,** 177–183. doi:10.3183/npprj-2007-22-02-p177-183 (2007).

53. *Lignins: occurrence, formation, structure and reactions.* (eds Sarkanen, K. V. & Ludwig, C. H.) 1–916 (Wiley Interscience, 1971).

54. Gellerstedt, G., Majtnerova, A. & Zhang, L. Towards a new concept of lignin condensation in kraft pulping. Initial results. *Comptes Rendus - Biologies* **327,** 817–826. doi:10.1016/j.crvi.2004.03.011 (2004).

55. Gierer, J. Chemical aspects of kraft pulping. *Wood Science and Technology* **14,** 241–266. doi:10.1007/BF00383453 (1980).

56. Sixta, H., Potthast, A. & Krotschek, A. W. in *Handbook of Pulp* (ed Sixta, H.) 109–509 (2006). doi:10.1002/9783527619887.ch4a.

57. Balakshin, M. Y., Capanema, E. A., Chen, C. L. & Gracz, H. S. Elucidation of the structures of residual and dissolved pine kraft lignins using an HMQC NMR technique. *Journal of agricultural and food chemistry* **51,** 6116–6127. doi:10.1021/JF034372D (2003).

58. Liitiä, T., Maunu, S. L., Sipilä, J. & Hortling, B. Application of solid-state 13C NMR spectroscopy and dipolar dephasing technique to determine the extent of condensation in technical lignins. *Solid State Nuclear Magnetic Resonance* **21,** 171–186. doi:10.1006/snmr.2002.0058 (2002).

59. Gellerstedt, G. & Lindfors, E.-L. On the formation of enol ether structures in lignin during kraft cooking. *Nordic Pulp & Paper Research Journal* **2,** 71–75. doi:10.3183/npprj-1987-02-02-p071-075 (1987).

60. Gellerstedt, G. in *Volume 2 Pulping Chemistry and Technology* (eds Ek, M., Gellerstedt, G. & Henriksson, G.) 91–120 (De Gruyter, Berlin, New York, 2009). doi:10.1515/9783110213423.91.

61. Dammström, S., Salmén, L. & Gatenholm, P. On the interactions between cellulose and xylan, a biomimetic simulation of the hardwood cell wall. *BioResources* **4,** 3–14. doi:10.15376/biores.4.1.3-14 (2009).

62. Sixta, H. in *Handbook of Pulp* (ed Sixta, H.) 21–68 (2006). doi:10.1002/3527608257.

63. McKibbins, S. Application of diffusion theory to the washing of kraft cooked wood chips. *TAPPI* **43,** 801–805 (1960).

64. Behr, E. A., Briggs, D. R. & Kaufert, F. H. Diffusion of dissolved materials through wood. *Journal of Physical Chemistry* **57,** 476–480. doi:10.1021/j150505a021 (1953).

65. Stone, J. E. & Scallan, A. M. Effect of component removal upon the porous structure of the cell wall of wood. *Journal of Polymer Science Part C: Polymer Symposia* **11,** 13–25. doi:10.1002/polc.5070110104 (1965).

66. Talton, J. H. & Cornell, R. H. Diffusion of sodium hydroxide in wood at high pH as a function of temperature and the extent of pulping. *Tappi journal* **70,** 115–118 (1987).

67. Stone, J. The effective capillary cross-sectional area of wood as a function of pH. *Tappi Journal* **40,** 539–541 (1957).

68. Jacobson, A. J. & Banerjee, S. Diffusion of tritiated water into water-saturated wood particles. *Holzforschung* **60,** 59–63. doi:10.1515/hf.2006.011 (2006).

69. Jakes, J. E. Mechanism for Diffusion through Secondary Cell Walls in Lignocellulosic Biomass. *Journal of Physical Chemistry B* **123,** 4333–4339. doi:10.1021/acs.jpcb.9b01430 (2019).

70. Cooper, P. A. Diffusion of Copper in Wood Cell Walls Following Vacuum Treatment. *Wood and Fiber Science* **30,** 382–395 (1998).

71. Ghaffari, R., Almqvist, H., Nilsson, R., Lidén, G. & Larsson, A. Mass Transport of Lignin in Confined Pores. *Polymers* **14,** 1993. doi:10.3390/POLYM14101993/S1 (2022).

72. Garver, T. M. & Callaghan, P. T. Hydrodynamics of Kraft Lignins. *Macromolecules* **24,** 420–430. doi:10.1021/ma00002a013 (1991).

73. Li, J. & Van Heiningen, A. R. *Diffusion of soluble lignin out of chips during magnesium bisulfite pulping* in *TAPPI Pulping/Process and Product Quality Conference* (2000), 908–916.

74. Zhao, X., Wu, R. & Liu, D. Evaluation of the mass transfer effects on delignification kinetics of atmospheric acetic acid fractionation of sugarcane bagasse with a shrinking-layer model. *Bioresource Technology* **261,** 52–61. doi:10.1016/j.biortech.2018.03.140 (2018).

75. Kawamata, Y. *et al.* Kinetic analysis of delignification of cedar wood during organosolv treatment with a two-phase solvent using the unreacted-core model. *Chemical Engineering Journal* **368,** 71–78. doi:10.1016/J.CEJ.2019.02.103 (2019).

76. Favis, B. D. *The leaching of lignin macromolecules from pulp fibres during washing* PhD thesis (McGill University, 1981).

77. Li, J., Phoenix, A. & Macleod, J. M. Diffusion of Lignin Macromolecules Within the Fibre Walls of Kraft Pulp. Part I: Determination of the Diffusion Coefficient under Alkaline Conditions. *Canadian Journal of Chemical Engineering* **75,** 16–22. doi:10.1002/cjce.5450750105 (1997).

78. Pahlevanzadeh, A. & Van Heiningen, A. A new look at the kinetics of oxygen delignification of softwood kraft pulp. *Holzforschung* **77,** 688–699. doi:10.1515/hf-2023-0045 (2023).

79. Ghaffari, R. *et al.* Effect of alkalinity on the diffusion of solvent-fractionated lignin through cellulose membranes. *Cellulose* **30,** 3685–3698. doi:10.1007/s10570-023-05098-8 (2023).

80. Norgren, M., Edlund, H. & Wågberg, L. Fundamental physical aspects on lignin dissolution. *Nordic Pulp and Paper Research Journal* **17,** 370–373. doi:10.3183/npprj-2002-17-04-p370-373 (2002).

81. Li, K. *Surface Lignin on Kraft Wood Pulp Fibres* PhD thesis (University of Toronto, 2003).

82. Hubbe, M., Alén, R., Paleologou, M., Kannangara, M. & Kihlman, J. Lignin recovery from spent alkaline pulping liquors using acidification, membrane separation, and related processing steps: A review. *BioResources* **14,** 2300–2351. doi:10.15376/biores.14.1.2300-2351 (2019).

83. Jara, R., Lawoko, M. & van Heiningen, A. Intrinsic dissolution kinetics and topochemistry of xylan, mannan, and lignin during auto-hydrolysis of red maple wood meal. *Canadian Journal of Chemical Engineering* **97,** 649–661. doi:10.1002/cjce.23373 (2019).

84. Evstigneev, E. I. Factors affecting lignin solubility. *Russian Journal of Applied Chemistry* **84,** 1040–1045. doi:10.1134/S1070427211060243 (2011).

85. Zhu, W., Westman, G. & Theliander, H. Lignin separation from kraft black liquor by combined ultrafiltration and precipitation: A study of solubility of lignin with different molecular properties. *Nordic Pulp and Paper Research Journal* **31,** 270–278. doi:10.3183/npprj-2016-31-02-p270-278 (2016).

86. Chambon, C. L. *et al.* Fractionation by Sequential Antisolvent Precipitation of Grass, Softwood, and Hardwood Lignins Isolated Using Low-Cost Ionic Liquids and Water. *ACS Sustainable Chemistry and Engineering* **8,** 3751–3761. doi:10.1021/acssuschemeng.9b06939 (2020).

87. Jiang, X. *et al.* Fractionation and Characterization of Kraft Lignin by Sequential Precipitation with Various Organic Solvents. *ACS Sustainable Chemistry and Engineering* **5,** 835–842. doi:10.1021/acssuschemeng.6b02174 (2017).

88. Evstigneyev, E. I. & Shevchenko, S. M. Structure, chemical reactivity and solubility of lignin: a fresh look. *Wood Science and Technology* **53,** 7–47. doi:10.1007/s00226-018-1059-1 (2019).

89. Lindström, T. The colloidal behaviour of kraft lignin - Part II. Coagulation of kraft lignin sots in the presence of simple and complex metal ions. *Colloid and Polymer Science Kolloid Zeitschrift & Zeitschrift für Polymere* **258,** 168–173. doi:10.1007/BF01498276 (1980).

90. Gierer, J. & Ljunggren, S. Reactions of lignin during sulfate pulping. Part 16. The kinetics of the cleavege of β-aryl ether linkages in structures containing carbonyl groups. *Sven Papperstidn* **82,** 71–81 (1979).

91. Gierer, J. & Ljunggren, S. The reactions of lignin during sulfate pulping Part 17. Kinetic treatment of the formation and competing reactions of quinone methide intermediates. *Svensk Papperstidning* **17,** 502 (1979).

92. Obst, J. R. Kinetics of Alkaline Cleavage of β-Aryl Ether Bonds in Lignin Models: Significance to Delignification. *Holzforschung* **37,** 23–28. doi:10.1515/hfsg.1983.37.1.23 (1983).

93. Olm, L. & Tistad, G. Kinetics of the initial stage of kraft pulping. *Svensk Papperstidning* **82,** 458–464 (1979).

94. Norden, S. & Teder, A. Modified Kraft Processes for Softwood Bleached-Grade Pulp. *Tappi* **62,** 49–51 (1979).

95. LeMon, S. & Teder, A. Kinetics of the delignification in kraft pulping. *Svensk Papperstidning* **11,** 407–414 (1973).

96. Chiang, V. L., Yu, J. & Eckert, R. C. Isothermal Reaction Kinetics of Kraft Delignification of Douglas-Fir. *Journal of Wood Chemistry and Technology* **10,** 293–310. doi:10.1080/02773819008050241 (1990).

97. Lindgren, C. T. & Lindström, M. E. The kinetics of residual delignification and factors affecting the amount of residual lignin during kraft pulping. *Journal of Pulp and Paper Science* **22,** 290–295 (1996).

98. Mansfield, S. D. & Weineisen, H. Wood fiber quality and kraft pulping efficiencies of trembling aspen (Populus tremuloides michx) clones. *Journal of Wood Chemistry and Technology* **27,** 135–151. doi:10.1080/02773810701700786 (2007).

99. Henriksson, G., Lawoko, M., Martin, M. E. E. & Gellerstedt, G. Lignin-carbohydrate network in wood and pulps: A determinant for reactivity. *Holzforschung* **61,** 668–674. doi:10.1515/hf.2007.097 (2007).

100. Antes, R. & Joutsimo, O. P. Effect of modified cooking on chemical composition of pulps from eucalyptus globulus and eucalyptus nitens. *BioResources* **10,** 210–226. doi:10.15376/biores.10.1.210-226 (2015).

101. Shimizu, S., Akiyama, T., Yokoyama, T. & Matsumoto, Y. Chemical Factors Underlying the More Rapid β-O-4 Bond Cleavage of Syringyl than Guaiacyl Lignin under Alkaline Delignification Conditions. *Journal of Wood Chemistry and Technology* **37,** 451–466. doi:10.1080/02773813.2017.1340957 (2017).

102. Kondo, R., Tsutsumi, Y. & Imamura, H. Kinetics of ß-Aryl Ether Cleavage of Phenolic Syringyl Type Lignin Model Compounds in Soda and Kraft Systems. *Holzforschung* **41,** 83–88. doi:10.1515/hfsg.1987.41.2.83 (1987).

103. Tsutsumi, Y., Kondo, R., Sakai, K. & Imamura, H. The Difference of Reactivity between Syringyl Lignin and Guaiacyl Lignin in Alkaline Systems. *Holzforschung* **49,** 423–428. doi:10.1515/hfsg.1995.49.5.423 (1995).

104. Pinto, P. C., Evtuguin, D. V. & Pascoal Neto, C. Effect of structural features of wood biopolymers on hardwood pulping and bleaching performance. *Industrial and Engineering Chemistry Research* **44,** 9777–9784. doi:10.1021/ie050760o (2005).

105. Del Río, J. C. *et al.* Determining the influence of eucalypt lignin composition in paper pulp yield using Py-GC/MS. *Journal of Analytical and Applied Pyrolysis* **74,** 110–115. doi:10.1016/j.jaap.2004.10.010 (2005).

106. Stewart, J. J., Kadla, J. F. & Mansfield, S. D. The influence of lignin chemistry and ultrastructure on the pulping efficiency of clonal aspen (Populus tremuloides Michx.) *Holzforschung* **60,** 111–122. doi:10.1515/hf.2006.019 (2006).

107. Guerra, A. *et al.* Influence of lignin structural features on eucalyptus globulus kraft pulping. *Industrial and Engineering Chemistry Research* **47,** 8542–8549. doi:10.1021/ie800320d (2008).

108. Almeida, D., B. Santos, R., W. Hart, P. & Jameel, H. Hardwood pulping kinetics of bulk and residual phases. *TAPPI Journal* **14,** 652–662. doi:10.32964/TJ14.10.652 (2015).

109. Ventorim, G., Alves, E. F., Penna, L. S. & Francis, R. C. Effect of S/G ratio on kraft pulping and ECF bleaching of some poplars and eucalyptus. *Cellulose Chemistry and Technology* **48,** 365–373 (2014).

110. Nicholson, D. J., Guilford, C. R., Abiola, A. B., Bose, S. K. & Francis, R. C. Estimation of the S/G ratios of the lignins in three widely used North American hardwoods. *Tappi Journal* **15,** 449–457. doi:10.32964/tj15.7.449 (2016).

111. Saltberg, A., Brelid, H. & Lundqvist, F. The effect of calcium on kraft delignification - Study of aspen, birch and eucalyptus. *Nordic Pulp and Paper Research Journal* **24,** 440–447. doi:10.3183/npprj-2009-24-04-p440-447 (2009).

112. Tolonen, L., Hiltunen, E., Helttunen, J. & Sixta, H. Effects of impregnation time on hardwood kraft pulp characteristics and papermaking potential – a mill study. *Tappi Journal,* 21–27. doi:10.32964/tj9.4.21 (2010).

113. Tavast, D. & Brännvall, E. Increased pulp yield by prolonged impregnation in softwood kraft pulping. *Nordic Pulp and Paper Research Journal* **32,** 14–20. doi:10.3183/npprj-2017-32-01-p014-020 (2017).

114. Santiago, A. S., Neto, C. P. & Vilela, C. Impact of effective alkali and sulfide profiling on Eucalyptus globulus kraft pulping. Selectivity of the impregnation phaseand its effect on final pulping results. *Journal of Chemical Technology and Biotechnology* **83,** 242–251. doi:10.1002/jctb.1799 (2008).

115. Kleppe, P. Kraft Pulping. *Tappi* **53,** 35–47 (1970).

116. Agarwal, N. & Gustafson, R. A Contribution to the Modeling of Kraft Pulping. *Canadian Journal of Chemical Engineering* **75,** 8–15. doi:10.1002/cjce.5450750104 (1997).

117. Dang, V. Q. & Nguyen, K. L. A universal kinetic model for characterisation of the effect of chip thickness on kraft pulping. *Bioresource Technology* **99,** 1486–1490. doi:10.1016/j.biortech.2007.02.034 (2008).

118. Tripathi, S. K., Mishra, O. P. & Bhardwaj, N. K. Effect of mixed hardwood chips thickness on unbleached and bleached pulp quality. *Journal of Scientific and Industrial Research* **77,** 516–519 (2018).

119. Wagih, A., Hasani, M., Hall, S. A. & Theliander, H. Micro/nano-structural evolution in spruce wood during soda pulping. *Holzforschung* **75,** 754–764. doi:10.1515/hf-2020-0113 (2021).

120. Andersson, R., Liden, J. & Ohman, L.-O. The Donnan theory applied to pulp washing - Experimental studies on the removal of anionic substances from an assumed fiber lumen volume and from the fiber wall. *Nordic Pulp & Paper Research Journal* **18,** 404–412. doi:10.3183/npprj-2003-18-04-p404-412 (2003).

121. Jara, R. *The Removal of Wood Components from Hardwood by Hot Water* PhD thesis (University of Maine, 2010).

122. Fearon, O., Kuitunen, S., Ruuttunen, K., Alopaeus, V. & Vuorinen, T. Detailed Modeling of Kraft Pulping Chemistry. Delignification. *Industrial and Engineering Chemistry Research* **59,** 12977–12985. doi:10.1021/acs.iecr.0c02110 (2020).

123. Dang, B. T. T. *On the Course of Kraft Cooking The impact of ionic strength* PhD thesis (Chalmers University of Technology, 2017).

124. Bogren, J., Brelid, H., Bialik, M. & Theliander, H. Impact of dissolved sodium salts on kraft cooking reactions. *Holzforschung* **63,** 226–231. doi:10.1515/hf.2009.032 (2009).

125. Kuitunen, S., Vuorinen, T. & Alopaeus, V. The role of Donnan effect in kraft cooking liquor impregnation and hot water extraction of wood. *Holzforschung* **67,** 511–521. doi:10.1515/hf-2012-0187 (2013).

126. Mcnaughton, J. G., Yean, W. Q. & Goring, D. a. I. Macro molecular properties of kraft lignins from spruce made soluble by a continuous flow process. *Tappi* **50,** 548–553 (1967).

127. Dang, B. T., Brelid, H. & Theliander, H. The impact of ionic strength on the molecular weight distribution (MWD) of lignin dissolved during softwood kraft cooking in a flow-through reactor. *Holzforschung* **70,** 495–501. doi:10.1515/hf-2015-0103 (2016).

128. Vroom, K. E. The" H" factor: a means of expressing cooking times and temperatures as a single variable. *PPMC* **58,** 228–231 (1957).

129. Hatton, J. V. Development of yield prediction equations in kraft pulping. *TAPPI* **56,** 97–100 (1973).

130. Teder, A. & Olm, L. Extended delignification by combination of modified kraft pulping and oxygen bleaching. *Paperi ja Puu* **63,** 315–316 (1981).

131. Gustafson, R. R., Sleicher, C. A., Mckean, W. T. & Flnlayson, B. A. Theoretical Model of the Kraft Pulping Process. *Industrial and Engineering Chemistry Process Design and Development* **22,** 87–96. doi:10.1021/i200020a016 (1983).

132. Blixt, J. & Gustavsson, C. A.-S. Temperature dependence of residual phase delignification during kraft pulping of softwood. *Nordic Pulp & Paper Research Journal* **15,** 12–17. doi:10.3183/npprj-2000-15-01-p012-017 (2000).

133. Smith, C. C. *Studies of the mathematical modelling, simulation, and control of the operation of a Kamyr continuous digester for the kraft process* PhD thesis (Purdue University, 1974).

134. Giudici, R. & Park, S. W. Kinetic model for kraft pulping of hardwood. *Industrial and Engineering Chemistry Research* **35,** 856–863. doi:10.1021/ie950341z (1996).

135. Santos, A., Rodríguez, F., Gilarranz, M. A., Moreno, D. & García-Ochoa, F. Kinetic Modeling of Kraft Delignification of Eucalyptus globulus. *Industrial and Engineering Chemistry Research* **36,** 4114–4125. doi:10.1021/ie9701940 (1997).

136. Gilarranz, M. A., Santos, A., García, J., Oliet, M. & Rodríguez, F. Kraft pulping of Eucalyptus globulus: Kinetics of residual delignification. *Industrial and Engineering Chemistry Research* **41,** 1955–1959. doi:10.1021/ie0108907 (2002).

137. Andersson, N., Wilson, D. I. & Germgård, U. An improved kinetic model structure for softwood kraft cooking. *Nordic Pulp & Paper Research Journal* **18,** 200–209. doi:10.3183/npprj-2003-18-02-p200-209 (2003).

138. Bogren, J., Brelid, H. & Theliander, H. Towards a general kraft delignification model. *Nordic Pulp and Paper Research Journal* **24,** 33–37. doi:10.3183/npprj-2009-24-01-p033-037 (2009).

139. Nieminen, K. & Sixta, H. Comparative evaluation of different kinetic models for batch cooking: A review. *Holzforschung* **66,** 791–799. doi:10.1515/hf-2011-0122 (2012).

140. Yang, L. & Liu, S. Kinetic model for Kraft pulping process. *Industrial and Engineering Chemistry Research* **44,** 7078–7085. doi:10.1021/ie050301n (2005).

141. Fearon, O. *et al.* Detailed modeling of the kraft pulping chemistry: carbohydrate reactions. *AIChE Journal* **66,** 16252. doi:10.1002/aic.16252 (2020).

142. Toivanen, T. J. & Alén, R. A FTIR/PLS method for determining variations in the chemical composition of birch (Betula pendula/B. pubescens) stem wood. *Appita Journal* **60,** 155–160 (2007).

143. Borrega, M., Niemela, K. & Sixta, H. Effect of hydrothermal treatment intensity on the formation of degradation products from birchwood. *Holzforschung* **67,** 871–879. doi:10.1515/hf-2013-0019 (2013).

144. Li, J., Kisara, K., Danielsson, S., Lindström, M. E. & Gellerstedt, G. An improved methodology for the quantification of uronic acid units in xylans and other polysaccharides. *Carbohydrate Research* **342,** 1442–1449. doi:10.1016/j.carres.2007.03.031 (2007).

145. Danielsson, S., Kisara, K. & Lindström, M. E. Kinetic study of hexenuronic and methylglucuronic acid reactions in pulp and in dissolved xylan during kraft pulping of hardwood. *Industrial and Engineering Chemistry Research* **45,** 2174–2178. doi:10.1021/ie051386v (2006).

146. Axelsson, P., Ek, M. & Teder, A. Influence of alkali profiling in birch kraft pulping on QPQP bleachability. *Nordic Pulp and Paper Research Journal* **19,** 37–43. doi:10.3183/npprj-2004-19-01-p037-043 (2004).

147. Lundgren, L. *et al.* Development of a new chemical method for distinguishing between Betula pendula and Betula pubescens in Sweden. *Canadian Journal of Forest Research* **25,** 1097–1102. doi:10.1139/x95-121 (1995).

148. Marion de Godoy, C., Hasani, M. & Theliander, H. Kraft pulping of model wood chips: local impact of process conditions on hardwood delignification and xylan retention. *Holzforschung* **78,** 446–458. doi:10.1515/hf-2024-0033 (2024).

149. Bogren, J., Brelid, H., Karlsson, S. & Theliander, H. Can the delignification rate be affected by previously applied cooking conditions? *Nordic Pulp and Paper Research Journal* **24,** 25–32. doi:10.3183/npprj-2009-24-01-p025-032 (2009).

150. Wojtasz-Mucha, J. *Pre-Extraction of Wood Components. Mild hydrothermal methods for a future materials biorefinery* PhD thesis (Chalmers University of Technology, 2020), 1–102.

151. Sluiter, A. *et al. Determination of structural carbohydrates and lignin in Biomass* tech. rep. April 2008 (NREL, Denver, 2012), 1–15.

152. Dence, C. W. in *Methods in Lignin Chemistry* (eds Lin, S. Y. & Dence, C. W.) 33–61 (Springer Berlin Heidelberg, Berlin, Heidelberg, 1992). doi:10.1007/978-3-642-74065-7.

153. Janson, J. Analytik der Polysaccharide in Holz und Zellstoff. *Faserforschung und Textiltechnik* **25,** 375–382 (1974).

154. Wojtasz-Mucha, J., Hasani, M. & Theliander, H. Hydrothermal pretreatment of wood by mild steam explosion and hot water extraction. *Bioresource Technology* **241,** 120–126. doi:10.1016/j.biortech.2017.05.061 (2017).

155. Lapierre, C. & Rolando, C. Thioacidolyses of Pre-Methylated Lignin Samples from Pine Compression and Poplar Woods. *Holzforschung* **42,** 1–4. doi:10.1515/hfsg.1988.42.1.1 (1988).

156. Orlowska, E. *et al.* β-: O -4 type dilignol compounds and their iron complexes for modeling of iron binding to humic acids: Synthesis, characterization, electrochemical studies and algal growth experiments. *New Journal of Chemistry* **41,** 11546–11555. doi:10.1039/c7nj02328f (2017).

157. Archibald, F., Bourbonnais, R., Jurasek, L., Paice, M. & Reid, I. Kraft pulp bleaching and delignification by Trametes versicolor. *Journal of Biotechnology* **53,** 215–236. doi:10.1016/S0168-1656(97)01675-1 (1997).

158. Giummarella, N., Lindén, P. A., Areskogh, D. & Lawoko, M. Fractional Profiling of Kraft Lignin Structure: Unravelling Insights on Lignin Reaction Mechanisms. *ACS Sustainable Chemistry and Engineering* **8,** 1112–1120. doi:10.1021/acssuschemeng.9b06027 (2020).

159. Borovkova, V. S. *et al.* Composition and Structure of Aspen (Pópulus trémula) Hemicelluloses Obtained by Oxidative Delignification. *Polymers* **14,** 4521. doi:10.3390/polym14214521 (2022).

160. Sable, I. *et al.* Chemical composition and fiber properties of fast-growing species in Latvia and its potential for forest bioindustry. *Forestry Studies* **66,** 27–32. doi:10.1515/fsmu-2017-0004 (2017).

161. Kotilainen, R., Alen, R. & Toivanen, T.-J. Chemical changes in black alder (alnus glutinosa) and european aspen (populus tremula) during heating at 150-200° in a nitrogen atmosphere. *Cellulose chemistry and technology* **35,** 275–284 (2001).

162. Kron, L., Hasani, M. & Theliander, H. Heterogenous Diffusion and Reaction Model of Kraft Delignification at the Cell Wall Level. *Industrial and Engineering Chemistry Research* **64,** 1497–1507. doi:10.1021/acs.iecr.4c03900 (2025).

163. Chiang, V. L., Puumala, R. J., Takeuchi, H. & Eckert, R. E. Comparison of softwood and hardwood kraft pulping. *Tappi journal* **71,** 173–176 (1988).

164. Shimizu, S., Yokoyama, T., Akiyama, T. & Matsumoto, Y. Reactivity of lignin with different composition of aromatic syringyl/guaiacyl structures and Erythro/Threo side chain structures in β-O-4 type during alkaline delignification: As a basis for the different degradability of hardwood and softwood lignin. *Journal of Agricultural and Food Chemistry* **60,** 6471–6476. doi:10.1021/jf301329v (2012).

165. Chiang, V. L. & Funaoka, M. The Dissolution and Condensation Reactions of Guaiacyl and Syringyl Units in Residual Lignin during Kraft Delignification of Sweetgum. *Holzforschung* **44,** 147–156. doi:10.1515/hfsg.1990.44.2.147 (1990).

166. Siau, J. F. Transport Processes in Wood. *Springer Series in Wood Science* **2.** doi:10.1007/978-3-642-69213-0 (1984).

167. Ahvazi, B. C. & Argyropoulos, D. S. Thermodynamic parameters governing the stereoselective degradation of arylglycerol-ß-aryl ether bonds in milled wood lignin under kraft pulping conditions. *Nordic Pulp and Paper Research Journal* **12,** 282–288. doi:10.3183/npprj-1997-12-04-p282-288 (1997).

168. Pinto, P. C., Evtuguin, D. V., Pascoal Neto, C. & Silvestre, A. J. D. Behavior of Eucalyptus globulus lignin during kraft pulping. I. Analysis by chemical degradation methods. *Journal of Wood Chemistry and Technology* **22,** 93–108. doi:10.1081/WCT-120013355 (2002).

169. Lourenço, A., Gominho, J., Marques, A. V. & Pereira, H. Variation of lignin monomeric composition during kraft pulping of Eucalyptus globulus heartwood and sapwood. *Journal of Wood Chemistry and Technology* **33,** 1–18. doi:10.1080/02773813.2012.703284 (2013).